# Gap Winds and their effects on regional oceanography Part II: Kodiak Island, Alaska

*Submitted to Deep Sea Research II*


Carol Ladd[1], Wei Cheng[1,2], and Sigrid Salo[1]

[1]Corresponding Author:
Carol Ladd
Pacific Marine Environmental Laboratory, NOAA
7600 Sand Point Way Seattle, WA, USA 98115-6349
Tel: (206) 526-6024
Fax: (206) 526-6485
Email: carol.ladd@noaa.gov

[2]Joint Institute for the Study of the Atmosphere and Ocean,
University of Washington, 3737 Brooklyn Ave NE, Box 355672,
Seattle, WA 98105-5672 USA
Email: wei.cheng@noaa.gov

## Abstract

Frequent gap winds, defined here as offshore-directed flow channeled through mountain gaps, have been observed near Kodiak Island in the Gulf of Alaska (GOA). Gap winds from the Iliamna Lake gap were investigated using QuikSCAT wind data. The influence of these wind events on the regional ocean was examined using satellite and *in situ* data combined with Regional Ocean Modeling System (ROMS) model runs. Gap winds influence the entire shelf width (> 200 km) northeast of Kodiak Island and extend an additional ~150 km off-shelf. Due to strong gradients in the along-shelf direction, they can result in vertical velocities in the ocean of over 20 m $d^{-1}$ due to Ekman pumping. The wind events also disrupt flow of the Alaska Coastal Current (ACC), resulting in decreased flow down Shelikof Strait and increased velocities on the outer shelf. This disruption of the ACC has implications for freshwater transport into the Bering Sea. The oceanographic response to gap winds may influence the survival of larval fishes as Arrowtooth Flounder recruitment is negatively correlated with the interannual frequency of gap-wind events, and Pacific Cod recruitment is positively correlated. The frequency of offshore directed winds exhibits a strong seasonal cycle averaging ~7 days per month during winter and ~2 days per month during summer. Interannual variability is correlated with the Pacific North America Index and shows a linear trend, increasing by 1.35 days per year. An accompanying paper discusses part I of our study (Ladd and Cheng, this issue) focusing on gap-wind events flowing out of Cross Sound in the eastern GOA.


## 1 Introduction

The Gulf of Alaska (GOA) has been called a “graveyard for storms” (Wilson and Overland, 1986). Winter storms in the North Pacific typically form east of Japan and cross the Pacific toward the Gulf of Alaska (GOA) (Rodionov et al., 2007; Rodionov et al., 2005; Wilson and Overland, 1986). The high coastal mountains surrounding the GOA impede the on-shore propagation of these storms, resulting in strong coastal pressure gradients and gale force winds. In addition, the contrast between relatively warm offshore water and cold continental air over Alaska during winter results in strong hydrostatic pressure gradients along the coast (Macklin et al., 1988). These conditions can result in barrier jets, gap winds, downslope winds, and interactions between them (i.e. Loescher et al., 2006; Winstead et al., 2006; Young and Winstead, 2004).

Gap winds, defined here as offshore-directed flow channeled through mountain gaps, form during conditions with high pressure over the interior and low pressure over the adjacent ocean. They have been examined in a number of observational and modeling studies, beginning with Reed's (1931) study of strong winds blowing out of the Strait of Juan de Fuca (~54°N, 130°W). Since that time, gap winds have been examined in many regions around the world. In the GOA, Synthetic Aperture Radar (SAR) data have shown strong gap winds in Prince William Sound (Liu et al., 2008), flowing out of Iliamna Lake northeast of Kodiak Island (Liu et al., 2006), and flowing out of Yakutat Bay and Cross Sound in Southeast Alaska (Ladd and Cheng, 2015; Loescher et al., 2006; Winstead et al., 2006).

In a study focused on Cook Inlet and Shelikof Strait, Liu et al. (2006) classify three channels within our region of interest through which gap-wind jets frequently blow: Puale Bay, Kaguyak, and Iliamna Lake (Fig. 1). These three jets often occur together, with over 60% of the Iliamna jets associated with Puale Bay and/or Kaguyak jets. They note that the Iliamna jets extend more than 200 km offshore from the mouth of Cook Inlet into the northern Gulf of Alaska (Liu et al., 2006). It has been suggested that the strong air-sea heat fluxes around Kodiak Island during the winter are largely due to these strong and frequent ageostrophic near-shore wind events (Janout et al., 2013).

Circulation in the GOA includes the cyclonic subarctic gyre in the basin and the Alaska Coastal Current (ACC) on the continental shelf (Fig. 1). The eastern boundary current of the subarctic gyre is the broad and variable Alaska Current. Eddies are regularly formed in the Alaska Current, with important consequences for fluxes of physical and chemical properties and biota (e.g. Atwood et al., 2010; Ladd et al., 2009; Ladd et al., 2007). Gap winds may be an important mechanism leading to the formation of eddies in the eastern GOA (Ladd and Cheng, 2015). At the head of the gulf, the gyre turns southwestward to form the Alaskan Stream, a western boundary current, tightly confined to the continental slope.

The ACC, a baroclinic coastal current driven by winds and freshwater, has been relatively well described in the northern and western GOA (e.g. Kowalik et al., 1994; Royer, 1981; Schumacher and Reed, 1986; Stabeno et al., 2004; Stabeno et al., this issue-a). Flowing southwestward along the Kenai Peninsula, it bifurcates when it reaches Kennedy-Stevenson Entrance with the majority of the current flowing down Shelikof Strait and a weaker flow along the seaward side of Kodiak Island (Schumacher et al., 1989; Stabeno et al., this issue-a; Stabeno et al., 1995). Flow along the Kenai Peninsula and the outer shelf seaward of Kodiak Island is strongly influenced by bathymetric steering by the canyons that incise the shelf-break there (Ladd et al., 2005b). The resulting cross-shelf transport of heat, salt, nutrients, and biota play an important role in the ecosystem of the region (Mordy et al., in progress). The along-shore ACC transports most of the extensive freshwater runoff that occurs along coastal Alaska. This freshwater transport may be critical to the freshwater budgets of the eastern Bering Sea shelf and the Arctic Ocean (Weingartner et al., 2005). Modeling studies show that the loss of freshwater from the ACC through offshore transport is enhanced under spatially varying wind conditions (Rogers-Cotrone et al., 2008; Yankovsky et al., 2010).

While gap winds and the conditions leading to them have been relatively well-described, their influence on the coastal ocean has been examined in only a few regions. Perhaps the most complete description of gap winds and their influence has been in the northeastern tropical Pacific. The gap winds associated with three mountain gaps in Central America have been shown to influence regional ocean circulation (Kessler, 2006), eddy formation (e.g. McCreary et al., 1989; Trasviña et al., 1995), and chlorophyll-*a* distributions (McClain et al., 2002). Liang et al. (2009) used satellite data to quantify the magnitude, duration and timing of anomalous ocean conditions associated with gap-wind events in this region.

This paper constitutes Part II of a two part study focusing on gap winds in the GOA. Part I focuses on gap winds flowing out of Cross Sound in the eastern GOA (Ladd and Cheng, 2015). Part II (this study) describes the frequency and variability of Iliamna gap winds and focuses on the influence of the winds on the regional oceanography. In both studies, our strategy is to use a combination of observations (satellite data and in situ measurements) and numerical experiments to both document gap-wind characteristics in these regions and to illustrate their influences on the regional oceanography. We treat the eastern and western GOA separately because the geographic layout (narrow shelf in the east versus wide shelf in the west), mean ocean circulation (eastern versus western boundary current systems), ecosystem response, and data availability are distinct between these two regions. We provide a summary comparing across the regions in the Summary and Discussion section.

# 2 Methods

## 2.1 Satellite data

QuikSCAT wind data (downloaded from the NOAA CoastWatch Program http://las.pfeg.noaa.gov/oceanWatch/) were used to quantify the seasonal and interannual frequency of wind events. The dataset includes daily averaged winds with 0.25° horizontal resolution. The SeaWinds instrument, on NASA's QuikSCAT satellite, is a dual-beam microwave scatterometer designed to estimate wind magnitude and direction over the global oceans at a reference height of 10 m above the surface. The QuikSCAT satellite offers daily coverage of 90% of the earth's oceans. QuikSCAT wind speeds are accurate to better than 2 m $s^{-1}$ and wind direction to better than 20°, comparable to *in situ* buoy measurements (Chelton et al., 2004; Freilich and Dunbar, 1999). QuikSCAT was launched in 1999 and its mission ended in November 2009. To examine Iliamna gap-wind jets near Kodiak Island, we focus on the region 58.5 – 59°N, 152 – 150.75°W . We call this region, the "Kodiak box" (see Fig. 1 for location of Kodiak box).

Another satellite-derived source of oceanic wind data at 10m is the ASCAT dataset (Verspeek et al., 2010). The ASCAT (Advanced Scatterometer) is flown aboard the European EUMETSAT MetOp-A and MetOp-B satellites. Data at 12.5 km and 25km resolution are available at JPL's PODAAC website; MetOp-A data start in March 2007 and MetOp-B data are available starting in November 2012. We used the 12.5km dataset (http://podaac.jpl.nasa.gov/dataset/ASCATA-L2-12.5km and /ASCATB-12.5km).

Because the swath width of the MetOp satellites is narrower than QuikSCAT, there are more days/regions with missing data, especially prior to the launch of MetOp-B. Thus, these data have not been compiled into a consistent daily average time series. They are used here as snapshots to illustrate recent individual events but are not used to examine the interannual time series of events as were QuikSCAT data.

Chlorophyll-*a* and SST were calculated from MODIS Aqua data obtained from NASA Goddard's Ocean Color website at http://oceancolor.gsfc.nasa.gov/. Processing is accomplished using the SeaWiFS Data Analysis System (SeaDAS) software (Fu et al., 1998; O'Reilly et al., 2000). The chlorophyll-*a* data are best used for feature identification and tracking. The actual value of the chlorophyll-*a* is somewhat controversial due to major differences when compared with that of the SeaWiFS sensor on Orbview-2. Both can differ substantially from high quality *in situ* measurements.

Sea surface height anomaly (SSHA) data were downloaded from AVISO (Archiving, Validation and Interpretation of Satellite Oceanographic data). The ‘‘all-sat-merged’’ dataset (obtained from http://www.aviso.altimetry.fr/) consists of delayed-mode, merged data from up to four satellites at a given time. AVISO applies an optimal interpolation methodology to merge data from multiple altimeters (Dibarboure et al., 2010; Le Traon et al., 1998). By using the maximum number of available satellites, sampling and long wavelength errors are improved, but the quality of the time series is not homogenous in time (Dibarboure et al., 2010). Merging data from multiple satellites with differing spatial and temporal resolution helps resolve mesoscale features, allowing for a better description of eddy activity (Ducet et al., 2000; Le Traon and Dibarboure, 2004; Pascual et al., 2006). Trajectories of mesoscale eddies have been derived from AVISO SSHA data by Chelton et. al (2011) using an automated procedure to identify and track eddies with lifetimes > 16 weeks. This dataset was downloaded from http://cioss.coas.oregonstate.edu/eddies/.

## 2.2 In situ data

Velocity data from moorings on the Gore Point line and in Kennedy-Stevenson Entrance are used to calculate transports. The Gore Point line included 3 moorings (GP32: 59.10°N, 151.00°W; GP34:

58.97°N, 150.95°W; and GP36: 58.75°N, 150.87°W) with upward looking 75 kHz acoustic Doppler current profilers (ADCP). The Kennedy-Stevenson Entrance line included one 75 kHz ADCP in Kennedy Entrance (59.02°N, 151.90°W) and one 300 kHz ADCP in Stevenson Entrance (58.77°N, 152.26°W). Time series of the velocity component normal to the mooring lines were used to compute the transport. Transports were low-pass filtered with a 35-hr, cosine-squared, tapered Lanczos filter to remove tidal and higher-frequency variability, and re-sampled at 6-hour intervals. These moorings are described in detail by (Stabeno et al., this issue-a).

## 2.3 Model

The Regional Ocean Modeling System (ROMS) is used to examine the effects of gap-wind events on the regional oceanography. A full description of ROMS can be found in (Haidvogel et al., 2008; Haidvogel et al., 2000; Shchepetkin and McWilliams, 1998; Shchepetkin and McWilliams, 2005), and references therein. The curvilinear horizontal coordinate of ROMS used in this study has a nominal resolution of 3 km and covers the entire GOA. It has 42 generalized terrain-following vertical layers. A multi-year integration of the 3-km GOA ROMS is described in Cheng et al. (2012).

For this study, we examine the results of a "control" experiment and a "gap-wind" experiment. Because the forcing for the gap-wind experiment is based on an event observed in January 2002, both experiments were initialized from the spun-up state of ROMS multi-year integration (Cheng et al., 2012) and run from 30 December 2001 to 14 March 2002. The lateral boundary conditions for both experiments are taken from the Simple Ocean Data Assimilation product (SODA, http://iridl.ldeo.columbia.edu/SOURCES/.CARTON-GIESE/.SODA/) version 2, 5-day averages. Additionally, sea surface elevation and currents derived from a tidal model (Foreman et al., 2000) are applied at the open boundaries in both experiments. These tidal signals are allowed to propagate freely throughout the model domain. Four diurnal (O1, Q1, P1, and K1) and four semidiurnal (N2, S2, K2, and M2) tidal constituents are used. In the control experiment, the surface forcing is from the Common Ocean-ice Reference Experiments (CORE, http://data1.gfdl.noaa.gov/nomads/forms/core/COREv2.html), and the forcing variables include daily surface downward longwave and shortwave radiation fluxes, 6-hourly surface air pressure, specific humidity, air temperature, and surface wind vectors, and monthly surface precipitation and river runoff. The horizontal resolution of the CORE forcing is approximately two degrees (~100 km in the GOA), and the forcing variables are interpolated onto the ROMS grid during model integration. In addition to atmospheric forcing, both experiments are driven by monthly freshwater runoff along the Alaskan coast with discharges from the Copper, Alsek, Stikine, Taku, and Susitna Rivers (Royer and Grosch, 2006). The runoff is applied as freshening on the topmost model layer. Total runoff along each segment of coastline is distributed with an exponential taper from the coastal point offshore, with an e-folding scale of 30 km.

Surface forcing in the gap-wind experiment is identical to the control experiment except that an idealized gap-wind event is imposed in the Kodiak Island region. The idealized gap-wind forcing is based on an event observed in January 2002. The maximum QuikSCAT wind speed on 24 January 2002 in the Kodiak Box was ~28 m $s^{-1}$ (Fig. 2a). The CORE forcing on this day exhibits a smoothed version of this event, with offshore winds (~315°T) with speeds ~20 m $s^{-1}$ throughout the region but no indication of the localized gap flow (Fig. 2b). The idealized gap-wind anomaly field (Fig. 2c) was created using a linear combination of two 2-dimensional elliptical Gaussian functions to approximate the positive wind jet northeast of Kodiak Island and the zone of weak winds in the area shielded by Kodiak Island (Table 1). The temporal evolution of the anomaly is created using a Gaussian function with decay scale of 3 days beginning on 15 January, peaking on 24 January, and ending on 2 February. The sum of the idealized gap-wind anomaly and the CORE forcing wind fields (Fig. 2d) was used to force the gap-wind model run. Modeled daily average fields with the tidal signal removed were analyzed.

# 3 Results

## 3.1 22 September 2013 event

To set the stage for a more general examination of the frequency and variability of gap-wind events near Kodiak Island and their effects on regional oceanography, we examine one particular event to the extent possible with a variety of types of data. ASCAT wind data show a strong gap-wind event beginning around 19 September, peaking on 22 September, and lasting until 24 September 2013. On 22 September, the winds are strongest (> 20 m $s^{-1}$) flowing from the Iliamna and Puale Bay gaps with weaker (~16 m $s^{-1}$) gap winds flowing from Kaguyak (Fig. 3). The Kaguyak gap wind is blocked by Kodiak Island, resulting in a region of lower wind speeds (8 – 10 m $s^{-1}$) over the shelf seaward of Kodiak Island.

MODIS sea surface temperature composited over 19 – 21 September (Fig. 4) shows relatively warm surface temperatures prior to the event (> 11°C almost everywhere surrounding Kodiak Island). On 23 September, after the peak of the winds, surface temperatures were < 10°C over much of the region surrounding Kodiak Island. The decrease of ~2° in ~3 days is likely primarily due to increased mixing associated with the strong winds. Note that outside of the influence of the gap winds (data available at the northeastern and southwestern edges of the image) (Fig. 4), SST did not change significantly.

MODIS chlorophyll (Fig. 5) shows high chlorophyll around Kennedy-Stevenson Entrance and northeastern Shelikof Strait prior to the event, and lower chlorophyll on the outer shelf. The region of higher (> 3 mg $m^{-3}$) offshelf chlorophyll (Fig. 5a) and lower (<10°C) SST (Fig. 4a) centered at ~ 57°N, 148°W is due to an eddy that has likely resulted in the transport of shelf waters off the shelf. During the event (23 September), chlorophyll is much reduced in Kennedy-Stevenson Entrance and northeastern Shelikof Strait, probably due to enhanced mixing removing phytoplankton from the surface. A streamer of higher chlorophyll is observed crossing the shelf offshore of Kodiak Island possibly due to increased cross-shelf transport suggested by the model results (see section 3.3). By 1 October after the event, chlorophyll levels near Kennedy-Stevenson Entrance have increased and levels on the outer shelf have decreased.

A true color picture shows dust blowing out over the GOA on 19 September (Fig. 6). These dust plumes have been shown to provide a source of bioavailable iron to the surface ocean, particularly in the autumn when riverbed sediments are most exposed (Crusius et al., 2011). Iron fertilization from an

August 2008 eruption of Kasatochi volcano in the Aleutian Islands is thought to have resulted in a widespread bloom within a few days after ashfall (Hamme et al., 2010) suggesting that phytoplankton are likely to respond quickly to iron input. The combination of iron input from dust and macronutrient input from mixing associated with the gap winds may provide for higher productivity in the days after an event, although it is impossible to attribute any of the surface chlorophyll features observed in Fig. 5 to dust input.

Altimetry data on the shelf has higher error than in the deep ocean due to proximity to land and errors in tidal corrections. We choose two locations (more than 50 km from land to minimize error) to examine the influence of the gap-wind event on SSHA. These points on either side of the wind field (57.9°N, 151.4°W; 58.6°N, 150.1°W; Fig. 1) are in locations where model SSHA suggests the largest differences due to the gap-wind event (see Section 3.4). Throughout the spring and summer of 2013, the SSHA at these two points have a magnitude <8 cm and track each other closely; differences between the two time series are mostly < 2 cm (Fig. 7). However, in mid-September, as the gap-wind event is spinning up, the SSHA at the two locations diverge from each other, increasing to the right of the winds and decreasing to the left of the winds, as suggested by model results. The difference between the two locations reaches a maximum > 13 cm, on 26 September (~4 days after the winds peak), comparable to SSHA differences seen in the model experiments. This pattern is due to Ekman convergences/divergences and suggests vertical circulations due to Ekman pumping. These vertical circulations can influence upwelling of nutrients into the euphotic zone and vertical transports of biota. In addition, cyclonic and anticyclonic eddies spin up on either side of the wind jet axis due to Ekman pumping. A similar response was observed in model runs of gap winds in the Gulfs of Tehuantepec and Papagayo off Central America (McCreary et al., 1989).

Mooring data at the Gore Point line (not shown) show transport increasing from a range of 0.6 – 1.2 Sv (1 Sv = $10^6$ m $s^{-1}$) during early September (1 – 21 September) to almost 2.2 Sv on September 22 – 23, consistent with model results (see Section 3.3). Unfortunately, the mooring in Kennedy Entrance failed on

22 September 2013 so we are not able to determine whether the gap-wind event resulted in decreased transport through Kennedy-Stevenson Entrance as suggested by model results.

## 3.2 Frequency and description of gap-wind events

Variability of the wind field in the Kodiak Island region is described using daily averaged QuikSCAT wind data. The large scale coastline angle is ~35/215° from north and offshore direction is ~125°T. Averaged over the Kodiak Box, winds are most frequently either easterly (75 – 105°T) or northwesterly (285 – 315°T) (Fig. 8). Almost 18% of the daily averaged winds (665 days out of 3747 total days) in the Kodiak Box are directed offshore (285 – 315°T; the highest frequency directional band). Offshore winds stronger than 10 m $s^{-1}$ occur approximately 13% of the total record.

The frequency of offshore winds exhibits a clear seasonal cycle, with the highest frequency of events in January and March (>7 days per month) and the lowest in June and July (~2 days per month) (Fig. 9). Strong winds occurred more often in the winter, with no events gale force or stronger in June, July, or August. December had the highest frequency of events gale force or stronger, with 35 events over the 10 year QuikSCAT record. Interannual variability in the number of offshore winds ranged from a low of 35 days in the winter of 2002/2003 to high of 60 days in 2005/2006. Interannual variability in the number of offshore wind days greater than or equal to gale force is significantly negatively correlated with the Pacific North America (PNA; Barnston and Livezey, 1987) index (R = –0.73, p-value = 0.017) and the Pacific Decadal Oscillation (PDO; Mantua et al., 1997) index (R = –0.64, p-value = 0.045). Correlations with other climate indices (North Pacific Index (Trenberth and Hurrell, 1994), Multivariate ENSO Index (Wolter and Timlin, 2011), North Pacific Gyre Oscillation (Di Lorenzo et al., 2009)) are not significant. In addition, the frequency of offshore wind days greater than or equal to gale force shows a significant linear trend (r=0.77, p-value=0.008), increasing by 1.35 days per year over the 1999 – 2009 QuikSCAT record.

To examine the spatial pattern associated with Iliamna gap-wind events, a composite was formed from the events with gale force or stronger wind speeds and separated from each other by more than 7 days (91 events; Fig. 10). The composite event shows the three local wind speed maxima associated with Puale Bay, Kaguyak, and Iliamna (identified by Liu et al. (2006)). The Puale Bay and Iliamna winds are very large scale, influencing the entire shelf width (> 200 km) and extending an additional ~150 km off-shelf. The Kaguyak winds are weaker and are blocked by Kodiak Island so they do not influence the outer shelf. The associated sea level pressure composite shows a low pressure system centered over the northern GOA (Fig. 10b). Janout et al. (2013) note that low pressure systems in this region are responsible for spatial variations in surface heat fluxes as northerly winds along the western side of the low bring cold continental air southward.

The spatially variable wind field results in Ekman pumping. As noted earlier, Ekman pumping can result in upwelling/downwelling of nutrients and biota in addition to contributing to the formation of eddies. In order to conserve mass, Ekman flux divergences result in a vertical velocity (Gill, 1982):

$$w_E = \frac{1}{\rho f}(\boldsymbol{\nabla} \times \boldsymbol{\tau})$$

where $f$ is the Coriolis parameter, $\rho$ is water density, and $\boldsymbol{\tau}$ is wind stress. During the 24 January 2002 Iliamna gap-wind event, associated Ekman pumping velocities calculated from QuikSCAT wind data exceeded 20 m $d^{-1}$ on the shelf northeast of Kodiak Island. During the winter months when gap-wind events are frequent, monthly climatological Ekman pumping velocities (calculated from 10 years of QuikSCAT data) can exceed 1.0 m $d^{-1}$ in a spatial pattern that is associated with gap winds (not shown).

## 3.3 Alaska Coastal Current

To examine the influence of the gap-wind event on circulation of the ACC, we calculate modeled transport along the mooring transects discussed by (Stabeno et al., this issue-a) (See fig. 1 for location of transects). While our model runs cover a short period of time (1 January 2002 – 14 March 2002), transports calculated from model results are within the range of variability observed over the many mooring deployments shown by (Stabeno et al., this issue-a; their Table 2). Transport across the shoreward portion (GAK1 – GAK4) of the Seward Line (east of the gap wind) shows almost no influence from the gap-wind event (Fig. 11). On the other hand, the flow through Kennedy-Stevenson Entrance (directly under the gap wind) is strongly affected by the gap-wind event. The gap-wind event results in transport through Kennedy-Stevenson Entrance that is reduced by 0.60 Sv (~40%) in the three days after the height of the event. The reduction in flow exceeds 10% for 10 days following the peak in the winds. Because of the large off-shelf component of flow directly under the path of the wind jet (Fig. 12), a compensatory onshore flow just to the northeast is enhanced. This onshore flow feeds enhanced transport across the Gore Point Line, which shows transport strengthening from 0.86 Sv in the control run to 1.30 Sv in the gap-wind run, a difference of 0.44 Sv or about 50% on the day after the height of the wind event (Fig. 11). The Gore Point transport remains more than 10% stronger for approximately 10 days after the height of the event. The combination of enhanced flow at the Gore Point Line and reduced flow through Kennedy-Stevenson Entrance implies that the coastal current is largely diverted to the seaward side of Kodiak Island with less flow down Shelikof Strait. Modeled transport across the Shelikof Strait Line shows a transport reduction of 0.43 Sv (more than 50% reduction) two days after the height of the gap-wind event. Transport down Shelikof Strait remains reduced by more than 10% for almost 3 weeks after the peak of the winds.

Modeled velocities on the shelf show the bifurcation of the ACC, with the majority flowing down Shelikof Strait and a weaker flow on the shelf seaward of Kodiak Island (Fig. 12). A comparison between the currents from the control run and the gap-wind run illustrate the influence of the gap-wind event. Three days after the peak gap wind speeds, the flow field is quite different in the two model runs (Fig. 12). In the absence of the gap-wind event (Fig. 12a), the ACC flows strongly down Shelikof Strait with maximum speeds over 0.50 m $s^{-1}$. In the gap-wind experiment, flow in Shelikof Strait is much weaker and flows on the outer shelf are stronger. The influence of the prominent bathymetry on the outer shelf is apparent with enhanced flow around the canyons. Throughout the water column, cross-shelf flow is stronger in the gap-wind model run than in the control run. The influence of the enhanced cross-shelf flow results in higher salinity in the canyons at depth (not shown).

Similar results are observed from mooring data. An Iliamna gap-wind event on 18 May 2013 is observed from ASCAT wind data. This event showed wind speed > 20 m $s^{-1}$ in the Iliamna region along with weaker (~16 m $s^{-1}$) gap flow from the Puale Bay and Kaguyak gaps (Fig. 13a). Transports increase at both the Gore Point and Kennedy-Stevenson Entrance moorings on 17 May as the winds are strengthening (Fig. 13b). After the initial increase, transports remain higher than earlier in May at the Gore Point moorings for at least 3 days before settling back to previous levels. On the other hand, transport at Kennedy-Stevenson Entrance drops quickly after the event, even changing direction to flow toward the outer shelf from 24 – 31 May. A similar ACC response is observed during a gap-wind event on 22 September 2013 (discussed previously), with increased transport at the Gore Point moorings during and after the event. Unfortunately, data are not available from the Kennedy Entrance mooring during this 2013 event to verify reduced flow through Kennedy-Stevenson Entrance.

## 3.4 Sea surface height

As the gap-wind event builds, the surface ocean is initially driven offshore under the offshore directed winds, resulting in negative sea surface height anomalies close to the coast (Fig. 14a). At the peak of the wind event, Ekman convergence/divergence results in low SSHA to the left and high SSHA to the right of the wind field with the strongest anomalies exhibited on the shelf. In the deeper water offshore of the shelf-break, weaker anomalies form (Fig. 14b). As the wind event begins to weaken, the SSHAs over the shelf decay rapidly, leaving behind localized positive and negative anomalies. In particular, a region of high SSHA remains near the northeast coast of Kodiak Island and small eddies with diameters of ~20-30 km (well resolved by the 3 km horizontal grid of the model) are apparent in Shelikof Strait (Fig. 14d,e). The small eddies (alternating high/low SSHA) in Shelikof Strait continue to form northeast of Kennedy-Stevenson Entrance, propagating southwestward through the Entrance and down the strait throughout the remainder of the model run (until 15 March). Similar eddies have been observed in Shelikof Strait (Bograd et al., 1994) and are thought to be important for walleye Pollock larval survival due to retention and enhanced feeding (Bailey et al., 1997; Napp et al., 1996; Schumacher et al., 1993).

The SSH anomalies in the deeper water offshore of the shelf-break continue to strengthen even after the winds weaken. The positive off-shelf anomaly (> 10 cm) on 10 February (Fig. 14e) represents a strengthening of an anticyclonic eddy that was already present prior to the gap-wind forcing.

Using a census of eddies derived from satellite SSHA data (Chelton et al., 2011), we examine the number of eddies formed in the region 54.5 – 57.5°N, 158 – 148°W during January – June of each year (not including eddies formed elsewhere and transiting through). The average over 2000 – 2010 is 1.6 eddies $yr^{-1}$ for anticyclonic eddies and 3.0 eddies $yr^{-1}$ for cyclonic eddies. The maximum number of anticyclonic eddies formed over that time period was 4 in 2008 with zero formed in 2000 and 2010. The number of anticyclonic eddies formed in the region is significantly correlated ($r=0.68$, p-value=0.03) with the total number of offshore wind events derived from QuikSCAT data. Correlations with the formation of cyclonic eddies are not significant.

# 4 Summary and discussion

## 4.1 Summary

Offshore winds are the most frequently observed wind direction in the region northeast of Kodiak Island (Kennedy-Stevenson Entrance). Strong gap winds flowing out of the gap in the mountainous terrain near Iliamna Lake are most common in the winter and are associated with low sea level pressure in the northern GOA. In the cross-shelf direction, they have large spatial scales, influencing the entire shelf width (> 200 km) and extending an additional ~150 km off-shelf. In the along-shelf direction, spatial scales are small and gradients are strong, leading to Ekman pumping velocities on the order of 20 m $d^{-1}$. These vertical velocities could lead to upwelling of nutrients and vertical movements of plankton.

Iliamna gap-wind events result in important changes in the circulation of the ACC, resulting in weaker flow down Shelikof Strait, and stronger flow on the outer shelf. Thus cross-shelf exchange is enhanced during gap-wind events. This could have important implications for freshwater transport. Model results suggest a reduction of ~ 25% in the transport down Shelikof Strait in the 3 weeks following a gap-wind event. A portion of the Shelikof Strait ACC flow remains near the coast as it flows westward toward the Aleutian Archipelago while the majority (~75%) flows downs the Shelikof Sea Valley to join the Alaskan Stream (Stabeno et al., this issue-a). It is unclear how a reduction of transport in Shelikof Strait would influence this partitioning of flow. Freshwater transport in the ACC may be critical to the freshwater budget of the eastern Bering Sea shelf and the Arctic Ocean (Weingartner et al., 2005). By transporting ACC water toward the outer shelf, gap-wind events may reduce the amount of freshwater flowing in the ACC and enhance the freshwater content in the Alaskan Stream. This diversion would change the pathway of that freshwater into the Bering Sea and ultimately the Arctic.

Correlations between the Seward Line and Gore Point transports calculated from mooring data are weaker than correlations between Gore Point, Kennedy/Stevenson Entrance, and Shelikof Strait (Stabeno et al., this issue-a). The model shows that a gap-wind event effects transport at Gore Point and Shelikof Strait but not at the Seward Line. Thus, gap-wind events may be an important mechanism disrupting the continuity of the ACC and contributing to weaker correlations between Gore Point and the Seward Line. Because the fate of the freshwater (to the Bering Sea shelf vs. the Alaskan Stream) may depend on gap winds, the Seward Line is likely not an ideal location to monitor those transports.

The number of gap-wind events each year shows a positive linear trend over the 10 year time series. The limited 10 year record, makes it impossible to determine whether this trend is due to climate change, decadal variability, or variability on some other time scale. Projections of future climate change due to $CO_2$ emissions show strong reductions in wintertime sea level pressure in the Bering Sea and western GOA over 2070 – 2090 (Walsh et al., 2013), suggesting increased storminess in the region. This could translate into more frequent gap-wind events, increasing mixing and cross-shelf exchange and perhaps changing the dominant flow of the ACC from primarily flowing down Shelikof Strait to more flow on the shelf seaward of Kodiak Island.

The number of gap-wind events each year shows negative correlations with the PNA and PDO indices. Climate models are able to reproduce the spatial and temporal variability of the PNA index

(Allan et al., 2014) suggesting that the frequency of gap-wind events under climate change may be forecastable.

## 4.2 Ecosystem implications

The overall goal of the Gulf of Alaska Integrated Ecosystem Research Program is to examine the physical and biological mechanisms that influence the survival of juvenile groundfishes in the GOA. The program focuses on five commercially and ecologically important groundfishes: Pacific Cod (*Gadus macrocephalus*), Walleye Pollock (*Gadus chalcogrammus*), Pacific Ocean Perch (*Sebastes alutus*), Sablefish (*Anoplopoma fimbria*), and Arrowtooth Flounder (*Atheresthes stomias*). Arrowtooth Flounder recruitment (Spies and Turnock, 2013) is negatively correlated with the number of Iliamna gap-wind events gale force or stronger during the spring (January – May) ($R = -0.75$, p-value = 0.0122, $n = 10$); Pacific Cod recruitment (A'mar and Palsson, 2013) is positively correlated with the number of Iliamna gap-wind events stronger than 10 m $s^{-1}$ during spring ($R = 0.76$, p-value = 0.0113, $n = 10$). The other three species (Walleye Pollock, Pacific Ocean Perch, and Sablefish) do not exhibit significant correlations with the frequency of Iliamna gap winds. If the number of gap-wind events in the region continues to increase, it could imply a trend toward unfavorable conditions for Arrowtooth Flounder and favorable conditions for Pacific Cod recruitment.

Arrowtooth Flounder larvae are most abundant in the western GOA from January through early March (Doyle and Mier, this issue) when gap-wind events are frequent. Eggs are found along the continental slope with evidence of movement of larvae onto the shelf during mid-February through mid-March. Larvae are found throughout the upper 200 m but ontogenetic migration toward the upper 50 m is evident (Doyle and Mier, this issue). The highest concentrations of larvae are associated with slope and shelf waters offshore of Amatuli Trough and Shelikof Sea Valley (Fig. 1), suggesting that these are primary regions of movement of larvae onto the shelf during spring (Doyle and Mier, this issue).

The negative correlation between the number of gap-wind events and Arrowtooth Flounder recruitment suggests that these wind events may influence the survival of Arrowtooth Flounder larvae. A negative relationship between Arrowtooth Flounder larval abundance and an index of winter wind mixing found by Doyle et al. (2009) suggests that the mixing associated with strong gap winds may negatively affect larval survival.  In addition, enhancement of off-shelf transport due to gap winds may negatively influence larval survival by impeding larval movement toward preferred shallower shelf waters.

Pacific Cod larvae are most abundant in April – May (later than Arrowtooth Flounder).  They are spawned on the shelf and their larval habitat is in shallower water than Arrowtooth Flounder (Doyle et al., 2009).  Doyle and Mier (this issue) note that early spring production of phytoplankton and microzooplankton may provide nourishment for the smallest Pacific Cod larvae.  Enhanced mixing and cross-shelf exchange during winter gap-wind events may provide the mix of nutrient (macro- and micro-) needed for early spring production that could be advantageous for Pacific Cod larval survival, explaining the positive correlation between the number of gap-wind events and Pacific Cod recruitment.

While the time series are short (10 years) and correlations may be spurious, the suggestion that the frequency of gap-wind events in this region may influence recruitment of some species is important and deserves further study.

### 4.3 Comparison with Cross Sound gap winds

The region near Cross Sound in the eastern GOA is another important region for the occurrence of gap-wind events (Ladd and Cheng, 2015).  The number of Cross Sound gap-wind events each year is correlated with the El Niño/Southern Oscillation and is uncorrelated with the number of Iliamna events.  This is not surprising as the low pressure system associated with Iliamna events (Fig. 10b) implies southerly to south-westerly geostrophic winds directed on-shore in the Cross Sound region.  While relationships were found between Arrowtooth Flounder and Pacific Cod recruitment and the frequency of Iliamna events, no significant correlations between Cross Sound gap winds and the recruitment of the five focal species were found.

Two effects of gap-wind events are clearly similar between the two regions:  gap winds disrupt the continuity of the ACC and enhance the formation of anticyclonic eddies.  However, in the eastern GOA, the ACC appears to be discontinuous at Cross Sound even in the absence of gap winds (Stabeno et al., this issue-b). In this region, while gap-wind flow may interfere with the continuity of ACC flow, the interaction of the ACC with flow and mixing in the Cross Sound estuary is probably more important (Ladd and Cheng, 2015; Stabeno et al., this issue-b). In the region around Kodiak Island, the ACC is more continuous than in the eastern GOA. In this region, gap-wind events are clearly important in the partitioning of ACC flow down Shelikof Strait vs. the outer shelf. This flow partition has implications for freshwater transport toward the Bering Sea, cross-shelf exchange on the outer shelf, and larval transport toward nursery grounds. The interaction of the enhanced cross-shelf exchange with the many canyons incising the shelf around Kodiak Island may be important to the flux of nutrients and larvae onto the shelf.

The region near Cross Sound is a primary formation region for GOA eddies and model results show that gap-wind events can result in eddy formation there (Ladd and Cheng, 2015). These eddies can influence the entire northern GOA, either moving westward into the basin or moving along the shelf-break toward the Kodiak Island region (Henson and Thomas, 2008; Ladd et al., 2005a; Ladd et al., 2007). Eddies sometimes form in the Kodiak Island region but more often, eddies observed near Kodiak Island have transited from the eastern GOA. Eddies are often observed to strengthen in the region near Kodiak Island. Many potential mechanisms could contribute to eddy modification in this region, including cross-shelf flow associated with canyons (Amatuli Trough and Shelikof Sea Valley) and western intensification of the boundary current. The prevalence of gap winds (both Iliamna and Puale Bay) may be an additional mechanism that could help explain the observed modification of eddies in this region.

## 5 Acknowledgments

QuikSCAT wind data were provided by the NOAA CoastWatch Program and Remote Sensing Systems, Inc. MODIS chlorophyll data were obtained from NOAA's CoastWatch Program and NASA's Goddard Space Flight Center, OceanColor Web. Discussions with Phyllis Stabeno, Nick Bond, and Al

Hermann are appreciated. This research is contribution 0826-RPP to NOAA's Ecosystems and Fisheries-Oceanography Coordinated Investigations, PMEL contribution 4227. This publication is partially funded by the Joint Institute for the Study of the Atmosphere and Ocean (JISAO) under NOAA Cooperative Agreement NA10OAR4320148, Contribution 2460. This is GOAIERP publication number 10 and NPRB publication #563, supported by the North Pacific Research Board through Projects G83 and G84.

## 6 Figure Captions

Figure 1. Map showing topography (color; m), schematic currents (white arrows), transport sections (black lines), Kodiak box (black square), and SSHA locations (black points). Note that, while the Seward Line moorings cross the shelf to the shelf-break, transport is only calculated over the shoreward portion of the line (GAK1 – GAK4) to focus on the ACC.

Figure 2. Wind forcing on 24 January 2002. Wind speed (m $s^{-1}$; color) is overlaid with wind vectors. Scale arrow (10 m $s^{-1}$) shown in panel (a). (a) Observed from QuikSCAT data; (b) Control run from CORE; (c) idealized gap-wind anomaly (difference between control run and gap-wind run); and (b) Gap-wind run (CORE forcing plus gap-wind forcing). White arrows on panel (c) denote direction of wind anomalies.

Figure 3. ASCAT wind data from 22 September 2013 with wind speed (m $s^{-1}$) denoted by color scale. Note that all winds around Kodiak Island are blowing in the offshore direction.

Figure 4. Sea surface temperature (°C) from MODIS composited over (a) 19 – 21 September 2013 and (b) 23 September 2013.

Figure 5. Chlorophyll *a* (mg $m^{-3}$) composites from MODIS for (a) 19 – 21 September 2013, (b) 23 September 2013, and (c) 1 October 2013.

Figure 6. True color image showing dust streams flowing out of Puale Bay, Kaguyak, and Iliamna gaps on 19 September 2013.

Figure 7. AVISO sea surface height anomalies (m) from two locations: 57.9°N, 151.4°W (black) and 58.6°N, 150.1°W (gray dashed) (top) and the difference (bottom).

Figure 8. Wind rose diagram of daily averaged QuikSCAT wind data in the region 58.5 – 59°N, 151 – 149.75°W illustrating frequency of occurrence in 12 directional and 3 wind speed bins. The plot was created from vector averaged wind direction and maximum wind speed. Wind direction is defined by meteorological convention as the direction from which the winds are blowing.

Figure 9. (a) Monthly histogram of all daily averaged winds averaged over 58.5 – 59°N, 151 – 149.75°W blowing from between 285 and 315°T. (b) Annual histogram of all daily averaged winds with a maximum wind speed in the region > 10 m $s^{-1}$ and blowing from between 285 and 315°T. PNA index is overlaid.

Figure 10. Composites derived from 91 gap-wind events separated from each other by more than 7 days and with regional, daily averaged wind speeds greater than or equal gale force (> 17.5 m $s^{-1}$). (a) Wind vectors (30 m $s^{-1}$ scale arrow shown in upper left corner) are overlaid on wind speed (color; m $s^{-1}$); (b) Sea level pressure from NCEP Reanalysis.

Figure 11. Difference in transports (Sv) calculated from the two model runs (gap-wind run – control run) across the 4 transects shown in Fig. 1. (a) Seward Line; (b) Gore Point Line, (c) Kennedy-Stevenson Entrance; (4) Shelikof Strait Line. Gray shaded area illustrates the timing of the gap-wind event. Vertical gray line shows the day of peak gap winds (24 January 2002). Thin horizontal line is zero difference.

Figure 12. Modeled current speed (color; m $s^{-1}$) and direction (black vectors) at the surface 3 days after peak of gap-wind event. (a) Control run; (b) Gap-wind run; (c) Difference (Gap-Control). Yellow arrows in (a) and (b) show the dominant flow patterns schematically. Flow in water deeper than 300 m is not shown for clarity.

Figure 13. (a) ASCAT wind speed (color; m $s^{-1}$) and direction on 18 May 2013. Locations of the Gore Point line (black) and Kennedy-Stevenson Entrance (red) are overlaid. (b) Transport ($m^3$ $s^{-1}$) calculated from moorings deployed along the Gore Point line (black) and the Kennedy-Stevenson Entrance (red).

Figure 14. Modeled sea surface height anomalies (gap-wind run – control run).

## 7 Tables

Table 1. Ellipses used to construct idealized gap-wind event used to force model (Fig. 2c).

| Center Latitude | Center Longitude | Major axis spatial scale | Minor axis spatial scale | Wind speed anomaly | Wind direction |
|---|---|---|---|---|---|
| 59.1°N | 152.8°W | 2.2° | 0.5° | 8 m $s^{-1}$ | 315°T |
| 57.9°N | 154.8°W | 2.2° | 0.5° | -12 m $s^{-1}$ | 315°T |

Table 2. Wind events with average wind direction between 285 and 315°T.

| Wind speed (m $s^{-1}$) | Number of events | Percentage of total offshore events |
|---|---|---|
| < 10 | 162 | 24 |
| 10 – 17.5 | 329 | 50 |
| 17.5 – 24.7 (gale) | 153 | 23 |
| 24.7 – 32.9 (storm) | 21 | 3 |
| > 32.9 (hurricane) | 0 | 0 |
| **Total** | **665** | **18 (of total days in record)** |

## 8 References

A'mar, T., Palsson, W., 2013. Assessment of the Pacific cod stock in the Gulf of Alaska. Stock Assessment and Fishery Evaluation Report for the Groundfish Resources of the Gulf of Alaska. North Pacific Fishery Management Council, Anchorage, AK.

Allan, A.M., Hostetler, S.W., Alder, J.R., 2014. Analysis of the present and future winter Pacific-North American teleconnection in the ECHAM5 global and RegCM3 regional climate models. Clim. Dyn. 42, 1671-1682. 10.1007/s00382-013-1910-x.

Atwood, E., Duffy-Anderson, J.T., Horne, J.K., Ladd, C., 2010. Influence of mesoscale eddies on ichthyoplankton assemblages in the Gulf of Alaska. Fish. Oceanogr. 19, 493-507. DOI: 10.1111/j.1365-2419.2010.00559.x.

Bailey, K.M., Stabeno, P.J., Powers, D.A., 1997. The role of larval retention and transport features in mortality and potential gene flow of walleye pollock. J. Fish Biol. 51, 135-154.

Barnston, A.G., Livezey, R.E., 1987. Classification, seasonality and persistence of low-frequency atmospheric circulation patterns. Mon. Wea. Rev. 115, 1083–1126.

Bograd, S.J., Stabeno, P.J., Schumacher, J.D., 1994. A census of mesoscale eddies in Shelikof Strait, Alaska, during 1989. J. Geophys. Res. - Oceans 99, 18243-18254.

Chelton, D.B., Schlax, M.G., Freilich, M.H., Milliff, R.F., 2004. Satellite measurements reveal persistent small-scale features in ocean winds. Science 303, 978-983. 10.1126/science.1091901.

Chelton, D.B., Schlax, M.G., Samelson, R.M., 2011. Global observations of nonlinear mesoscale eddies. Prog. Oceanogr. 91, 167-216 doi:10.1016/j.pocean.2011.01.002.

Cheng, W., Hermann, A.J., Coyle, K.O., Dobbins, E.L., Kachel, N.B., Stabeno, P.J., 2012. Macro- and micro-nutrient flux to a highly productive submarine bank in the Gulf of Alaska: A model-based analysis of daily and interannual variability. Prog. Oceanogr. 101, 63-77. 10.1016/j.pocean.2012.01.001.

Crusius, J., Schroth, A.W., Gassó, S., Moy, C.M., Levy, R.C., Gatica, M., 2011. Glacial flour dust storms in the Gulf of Alaska: Hydrologic and meteorological controls and their importance as a source of bioavailable iron. Geophys. Res. Lett. 38, L06602. 10.1029/2010gl046573.

Di Lorenzo, E., Fiechter, J., Schneider, N., Bracco, A., Miller, A.J., Franks, P.J.S., Bograd, S.J., Moore, A.M., Thomas, A.C., Crawford, W., Pena, A., Hermann, A.J., 2009. Nutrient and salinity decadal variations in the central and eastern North Pacific. Geophys. Res. Lett. 36. L14601, 10.1029/2009gl038261.

Dibarboure, G., Lauret, O., Mertz, F., Rosmorduc, V., Maheu, C., 2010. SSALTO/DUACS User Handbook : (M)SLA and (M)ADT Near-Real Time and Delayed Time Products. AVISO, Ramonville St-Agne, France.

Doyle, M.J., Mier, K.L., this issue. Early life history pelagic exposure profiles of selected commercially important fish species in the Gulf of Alaska. Deep-Sea Res. II.

Doyle, M.J., Picquelle, S.J., Mier, K.L., Spillane, M.C., Bond, N.A., 2009. Larval fish abundance and physical forcing in the Gulf of Alaska, 1981-2003. Prog. Oceanogr. 80, 163-187. 10.1016/j.pocean.2009.03.002.

Ducet, N., Le Traon, P.Y., Reverdin, G., 2000. Global high-resolution mapping of ocean circulation from TOPEX/Poseidon and ERS-1 and-2. J. Geophys. Res. - Oceans 105, 19477-19498.

Foreman, M.G.G., Crawford, W.R., Cherniawsky, J.Y., Henry, R.F., Tarbotton, M.R., 2000. A high-resolution assimilating tidal model for the northeast Pacific Ocean. J. Geophys. Res. - Oceans 105, 28629-28651.

Freilich, M.H., Dunbar, R.S., 1999. The accuracy of the NSCAT 1 vector winds: Comparisons with National Data Buoy Center buoys. J. Geophys. Res. 104, 11231-11246. 10.1029/1998jc900091.

Fu, G., Baith, K.S., McClain, C.R., 1998. SeaDAS: The SeaWiFS Data Analysis System. Proceedings of The 4th Pacific Ocean Remote Sensing Conference, Qingdao, China, 73-79.

Gill, A.E., 1982. Atmosphere-ocean dynamics. Academic Press, New York.

Haidvogel, D.B., Arango, H.G., Budgell, W.P., Cornuelle, B.D., Curchitser, E.N., Di Lorenzo, E., Fennel, K., Geyer, W.R., Hermann, A.J., Lanerolle, L., Levin, J., McWilliams, J.C., Miller, A.J., Moore, A.M., Powell, T.M., Shchepetkin, A.G., Sherwood, C.R., Signell, R.P., Warner, J.C., Wilkin, J., 2008. Ocean forecasting in terrain-following coordinates: Formulation and skill assessment of the Regional Ocean Modeling System. Journal of Computational Physics 227, 3595-3624.

Haidvogel, D.B., Arango, H.G., Hedstrom, K., Beckmann, A., Malanotte-Rizzoli, P., Shchepetkin, A.G., 2000. Model evaluation experiments in the North Atlantic Basin: simulations in nonlinear terrain-following coordinates. Dyn. Atmos. Ocean. 32, 239-281.

Hamme, R.C., Webley, P.W., Crawford, W.R., Whitney, F.A., DeGrandpre, M.D., Emerson, S.R., Eriksen, C.C., Giesbrecht, K.E., Gower, J.F.R., Kavanaugh, M.T., Pena, M.A., Sabine, C.L., Batten, S.D., Coogan, L.A., Grundle, D.S., Lockwood, D., 2010. Volcanic ash fuels anomalous plankton bloom in subarctic northeast Pacific. Geophys. Res. Lett. 37, L19604. 10.1029/2010gl044629.

Henson, S.A., Thomas, A.C., 2008. A census of oceanic anticyclonic eddies in the Gulf of Alaska. Deep-Sea Res. I 55, 163-176 doi:10.1016/j.dsr.2007.11.005.

Janout, M.A., Weingartner, T.J., Stabeno, P.J., 2013. Air-sea and oceanic heat flux contributions to the heat budget of the northern Gulf of Alaska shelf. Journal of Geophysical Research: Oceans 118, 1807-1820. 10.1002/jgrc.20095.

Kessler, W.S., 2006. The circulation of the eastern tropical Pacific: A review. Prog. Oceanogr. 69, 181-217.

Kowalik, Z., Luick, J.L., Royer, T.C., 1994. On the dynamics of the Alaska Coastal Current. Cont. Shelf Res. 14, 831-845.

Ladd, C., Cheng, W., 2015. Gap winds and their effects on regional oceanography Part I: Cross Sound, Alaska. Deep-Sea Res. II. doi:10.1016/j.dsr2.2015.08.005.

Ladd, C., Crawford, W.R., Harpold, C.E., Johnson, W.K., Kachel, N.B., Stabeno, P.J., Whitney, F., 2009. A synoptic survey of young mesoscale eddies in the Eastern Gulf of Alaska. Deep-Sea Res. II 56, 2460–2473. doi:10.1016/j.dsr2.2009.02.007.

Ladd, C., Kachel, N.B., Mordy, C.W., Stabeno, P.J., 2005a. Observations from a Yakutat eddy in the northern Gulf of Alaska. J. Geophys. Res. - Oceans 110, C03003. doi: 10.1029/2004JC002710.

Ladd, C., Mordy, C.W., Kachel, N.B., Stabeno, P.J., 2007. Northern Gulf of Alaska eddies and associated anomalies. Deep-Sea Res. I 54, 487-509. doi:10.1016/j.dsr.2007.01.006.

Ladd, C., Stabeno, P., Cokelet, E.D., 2005b. A note on cross-shelf exchange in the northern Gulf of Alaska. Deep-Sea Res. II 52, 667-679.

Le Traon, P.Y., Dibarboure, G., 2004. An illustration of the contribution of the TOPEX/Poseidon-Jason-1 tandem mission to mesoscale variability studies. Marine Geodesy 27, 3-13.

Le Traon, P.Y., Nadal, F., Ducet, N., 1998. An improved mapping method of multi-satellite altimeter data. J. Atmos. Oceanic Technol. 15, 522-534.

Liang, J.-H., McWilliams, J.C., Gruber, N., 2009. High-frequency response of the ocean to mountain gap winds in the northeastern tropical Pacific. J. Geophys. Res. - Oceans 114. C12005, doi:10.1029/2009JC005370.

Liu, H., Olsson, P.Q., Volz, K.P., Yi, H., 2006. A climatology of mesoscale model simulated low-level wind jets over Cook Inlet and Shelikof Strait, Alaska. Estuarine, Coastal and Shelf Science 70, 551-566. 10.1016/j.ecss.2006.06.011.

Liu, H.B., Olsson, P.Q., Volz, K., 2008. SAR observation and modeling of gap winds in the Prince William Sound of Alaska. Sensors 8, 4894-4914. 10.3390/s8084894.

Loescher, K.A., Young, G.S., Colle, B.A., Winstead, N.S., 2006. Climatology of barrier jets along the Alaskan coast. Part 1: Spatial and temporal distributions. Mon. Wea. Rev. 134, 437-453.

Macklin, S.A., Lackmann, G.M., Gray, J., 1988. Offshore-directed winds in the vicinity of Prince William Sound, Alaska. Mon. Wea. Rev. 116, 1289-1301.

Mantua, N.J., Hare, S.R., Zhang, Y., Wallace, J.M., Francis, R.C., 1997. A Pacific interdecadal climate oscillation with impacts on salmon production. Bull. Amer. Meteor. Soc. 78, 1069-1079.

McClain, C.R., Christian, J.R., Signorini, S.R., Lewis, M.R., Asanuma, I., Turk, D., Dupouy-Douchement, C., 2002. Satellite ocean-color observations of the tropical Pacific Ocean. Deep-Sea Res. II 49, 2533-2560. doi: 10.1016/s0967-0645(02)00047-4.

McCreary, J.P., Lee, H.S., Enfield, D.B., 1989. The response of the coastal ocean to strong offshore winds: With application to circulations in the Gulfs of Tehuantepec and Papagayo. J. Mar. Res. 47, 81-109.

Mordy, C.W., Stabeno, P.J., Kachel, N.B., Kachel, D., Ladd, C., Zimmerman, M., Doyle, M., in progress. Importance of canyons to the northern Gulf of Alaska ecosystem. Deep-Sea Res. II.

Napp, J., Incze, L., Ortner, P., Siefert, D., Britt, L., 1996. The plankton of Shelikof Strait, Alaska: Standing stock, production, mesoscale variability and their relevance to larval fish survival. Fish. Oceanogr. 5, 19-38.

O'Reilly, J.E., Maritorena, S., Siegel, D.A., O'Brien, M.C., Toole, D., Chavez, F.P., Strutton, P., G.F. Cota, S.B. Hooker, C.R. McClain, K.L. Carder, F. Muller-Karger, L. Harding, A. Magnuson, D. Phinney, G.F. Moore, J. Aiken, K.R. Arrigo, R. Letelier, Culver, M., 2000. Ocean Chlorophyll a Algorithms for SeaWiFS, OC2, and OC4: Version 4. In: O'Reilly, J.E., 24 Coauthors (Eds.), SeaWiFS Postlaunch Calibration and Validation Analyses, Part 3, NASA Tech. Memo. 2000-206892. NASA Goddard Space Flight Center, Greenbelt, MD, pp. 9-19.

Pascual, A., Faugère, Y., Larnicol, G., Le Traon, P.Y., 2006. Improved description of the ocean mesoscale variability by combining four satellite altimeters. Geophys. Res. Lett. 33, L02611. doi:10.1029/2005GL024633.

Reed, T.R., 1931. Gap winds of the Strait of Juan de Fuca. Mon. Wea. Rev. 59, 373-376. 10.1175/1520-0493(1931)59<373:gwotso>2.0.co;2.

Rodionov, S.N., Bond, N.A., Overland, J.E., 2007. The Aleutian Low, storm tracks, and winter climate variability in the Bering Sea. Deep-Sea Res. II 54, 2560-2577.

Rodionov, S.N., Overland, J.E., Bond, N.A., 2005. Spatial and temporal variability of the Aleutian climate. Fish. Oceanogr. 14, 3-21. doi:10.1111/j.1365-2419.2005.00363.x.

Rogers-Cotrone, J., Yankovsky, A.E., Weingartner, T.J., 2008. The impact of spatial wind variations on freshwater transport by the Alaska Coastal Current. J. Mar. Res. 66, 899-925.

Royer, T.C., 1981. Baroclinic transport in the Gulf of Alaska Part II. A fresh-water driven coastal current. J. Mar. Res. 39, 251-266.

Royer, T.C., Grosch, C.E., 2006. Update of a freshwater discharge model for the Gulf of Alaska, North Pacific Research Board Final Report 734, 12 p.

Schumacher, J.D., Reed, R.K., 1986. On the Alaska Coastal Current in the Western Gulf of Alaska. J. Geophys. Res. - Oceans 91, 9655-9661.

Schumacher, J.D., Stabeno, P.J., Bograd, S.J., 1993. Characteristics of an eddy over a continental shelf: Shelikof Strait, Alaska. J. Geophys. Res. - Oceans 98, 8395-8404.

Schumacher, J.D., Stabeno, P.J., Roach, A.T., 1989. Volume transport in the Alaska Coastal Current. Cont. Shelf Res. 9, 1071-1083.

Shchepetkin, A.F., McWilliams, J.C., 1998. Quasi-Monotone Advection Schemes Based on Explicit Locally Adaptive Dissipation. Mon. Wea. Rev. 126, 1541-1580. 10.1175/1520-0493(1998)126<1541:QMASBO>2.0.CO;2.

Shchepetkin, A.G., McWilliams, J.C., 2005. The Regional Ocean Modeling System (ROMS): A split-explicit, free-surface, topography-following coordinates ocean model. Ocean Modelling 9, 347-404.

Spies, I., Turnock, B.J., 2013. Assessment of the arrowtooth flounder stock in the Gulf of Alaska. Stock Assessment and Fishery Evaluation Report for the Groundfish Resources of the Gulf of Alaska. North Pacific Fishery Management Council, Anchorage, AK.

Stabeno, P., Bond, N.A., Hermann, A.J., Kachel, N.B., Mordy, C.W., Overland, J.E., 2004. Meteorology and oceanography of the northern Gulf of Alaska. Cont. Shelf Res. 24, 859-897.

Stabeno, P.J., Bell, S., Cheng, W., Danielson, S., Kachel, N.B., Mordy, C.W., this issue-a. Long-term observations of Alaska Coastal Current in the northern Gulf of Alaska. Deep-Sea Res. II.

Stabeno, P.J., Bond, N.A., Kachel, N.B., Ladd, C., Mordy, C., Strom, S.L., this issue-b. Southeast Alaskan shelf from southern tip of Baranof Island to Kayak Island: Currents, mixing and chlorophyll-*a*. Deep-Sea Res. II.

Stabeno, P.J., Reed, R.K., Schumacher, J.D., 1995. The Alaska Coastal Current: Continuity of transport and forcing. J. Geophys. Res. 100, 2477-2485.

Trasviña, A., Barton, E.D., Brown, J., Velez, H.S., Kosro, P.M., Smith, R.L., 1995. Offshore wind forcing in the Gulf of Tehuantepec, Mexico: The asymmetric circulation. J. Geophys. Res. 100, 20649-20663. doi: 10.1029/95jc01283.

Trenberth, K.E., Hurrell, J.W., 1994. Decadal atmosphere-ocean variations in the Pacific. Clim. Dyn. 9, 303-319.

Verspeek, J.A., Stoffelen, A., Portabella, M., Bonekamp, H., Anderson, C., Figa, J., 2010. Validation and calibration of ASCAT using CMOD5.n. IEEE Transactions on Geoscience and Remote Sensing 48, 386-395. doi:10.1109/TGRS.2009.2027896.

Walsh, J.E., Park, H., Chapman, W.L., Ohata, T., 2013. Relationships between variations of the land-ocean-atmosphere system of northeastern Asia and northwestern North America. Polar Science 7, 188-203. 10.1016/j.polar.2013.05.002.

Weingartner, T.J., Danielson, S.L., Royer, T.C., 2005. Freshwater variability and predictability in the Alaska Coastal Current. Deep-Sea Res. II 52, 169-191. DOI: 10.1016/j.dsr2.2004.09.030.

Wilson, J.G., Overland, J.E., 1986. Meteorology. In: Hood, D.W., Zimmerman, S.T. (Eds.), The Gulf of Alaska, Physical Environment and Biological Resources. U.S. Department of Commerce, National Oceanic and Atmospheric Administration, National Ocean Service, Office of Oceanography and Marine Assessment, Ocean Assessments Division, Alaska Office p. 655.

Winstead, N.S., Colle, B.A., Bond, N.A., Young, G., Olson, J., Loescher, K., Monaldo, F., Thompson, D., Pichel, W., 2006. Using SAR remote sensing, field observations, and models to better understand coastal flows in the Gulf of Alaska. Bull. Amer. Meteor. Soc. 87, 787–800

Wolter, K., Timlin, M.S., 2011. El Niño/Southern Oscillation behaviour since 1871 as diagnosed in an extended multivariate ENSO index (MEI.ext). International Journal of Climatology 31, 1074-1087. 10.1002/joc.2336.

Yankovsky, A.E., Maze, G.M., Weingartner, T.J., 2010. Offshore transport of the Alaska Coastal Current water induced by a cyclonic wind field. Geophys. Res. Lett. 37. 10.1029/2009gl041939.

Young, G., Winstead, N., 2004. Meteorological phenomena in high resolution SAR wind imagery, in: Beal, B., Young, G., Monaldo, F., Thompson, D., Winstead, N., Scott, C. (Eds.), High Resolution Wind Monitoring with Wide Swath SAR: A User's Guide, 13-31 p.

# 9 Web References

AVISO, http://www.aviso.altimetry.fr/en/home.html, last accessed April 2015.

Chelton, D.B. and Schlax, M.G., Mesoscale eddies in altimeter observations of SSH. http://cioss.coas.oregonstate.edu/eddies/, last accessed July 2013.

Common Ocean-ice Reference Experiments (CORE), http://data1.gfdl.noaa.gov/nomads/forms/core/COREv2.html, last accessed April 2012.

MetOp-A ASCAT Level 2 12.5km Ocean Surface Wind Vectors, http://podaac.jpl.nasa.gov/dataset/ASCATA-L2-12.5km, last accessed January 2015.

MetOp-B ASCAT Level 2 Ocean Surface Wind Vectors Optimized for Coastal Ocean, http://podaac.jpl.nasa.gov/dataset/ASCATB-L2-Coastal, last accessed January 2015.

NOAA CoastWatch Program webpage, http://las.pfeg.noaa.gov/oceanWatch/, last accessed April 2015.

NOAA Coastwatch QuikSCAT webpage, http://coastwatch.pfeg.noaa.gov/infog/QN_ux10_las.html, last accessed April 2015.

NASA OceanColor Web webpage, http://oceancolor.gsfc.nasa.gov/, last accessed January 2015.

Simple Ocean Data Assimilation product (SODA, http://iridl.ldeo.columbia.edu/SOURCES/.CARTON-GIESE/.SODA/), last accessed April 2012.

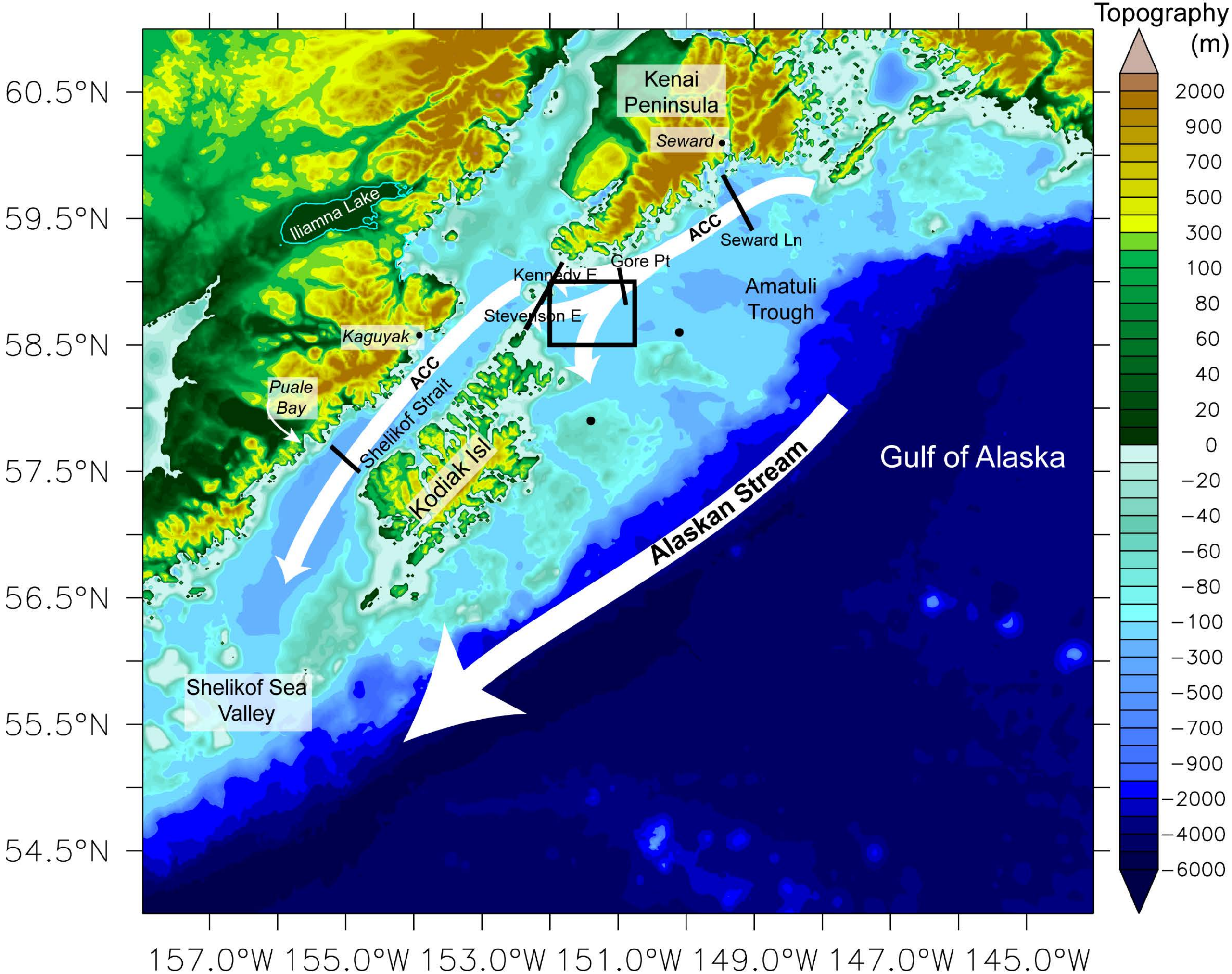

Topography (m)
2000
900
700
500
300
100
80
60
40
20
0
-20
-40
-60
-80
-100
-300
-500
-700
-900
-2000
-4000
-6000
60.5°N
59.5°N
58.5°N
57.5°N
56.5°N
55.5°N
54.5°N
157.0°W
155.0°W
153.0°W
151.0°W
149.0°W
147.0°W
145.0°W
Kenai Peninsula
Seward
Iliamna Lake
ACC
Seward Ln
Gore Pt
Kennedy E
Stevenson E
Amatuli Trough
Kaguyak
ACC
Puale Bay
Shelikof Strait
Kodiak Isl
Alaskan Stream
Gulf of Alaska
Shelikof Sea Valley


Fig. 1

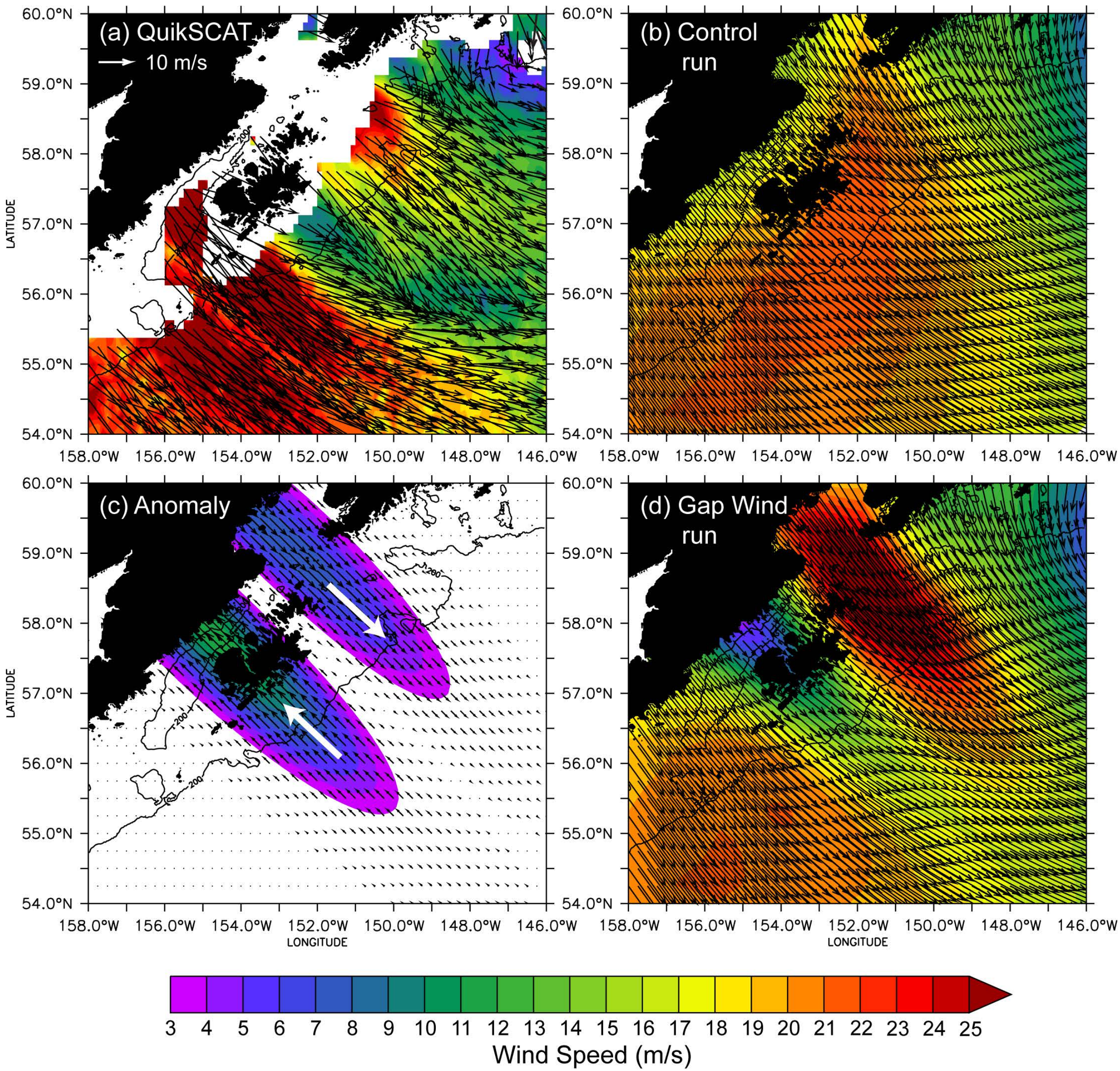
(a) QuikSCAT
10 m/s
(b) Control run
(c) Anomaly
(d) Gap Wind run
60.0°N
59.0°N
58.0°N
57.0°N
56.0°N
55.0°N
54.0°N
LATITUDE
158.0°W
156.0°W
154.0°W
152.0°W
150.0°W
148.0°W
146.0°W
LONGITUDE
200
3 4 5 6 7 8 9 10 11 12 13 14 15 16 17 18 19 20 21 22 23 24 25
Wind Speed (m/s)

Fig. 2

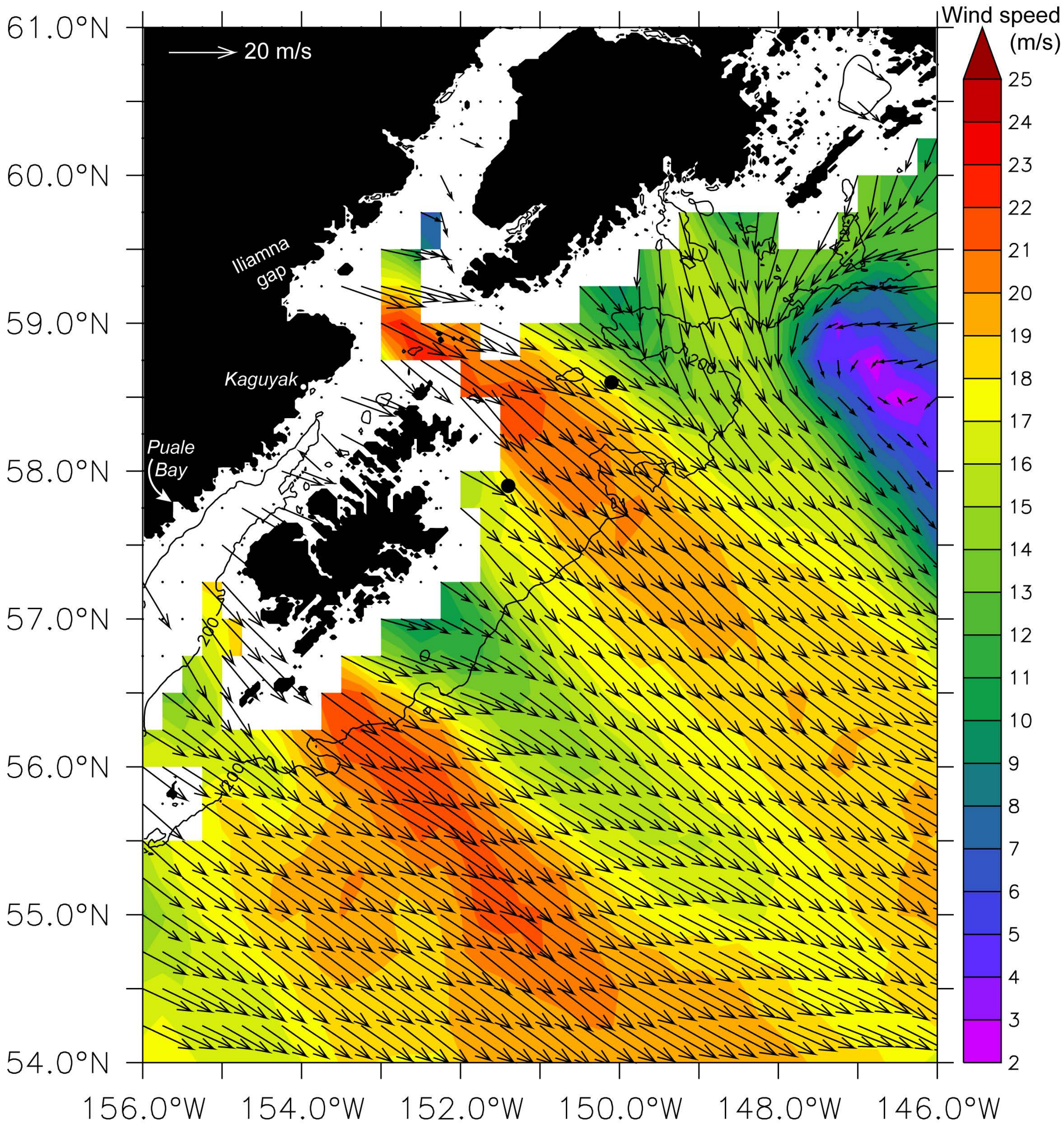

61.0°N
60.0°N
59.0°N
58.0°N
57.0°N
56.0°N
55.0°N
54.0°N
156.0°W
154.0°W
152.0°W
150.0°W
148.0°W
146.0°W
20 m/s
Iliamna gap
Kaguyak
Puale Bay
200
Wind speed (m/s)
25
24
23
22
21
20
19
18
17
16
15
14
13
12
11
10
9
8
7
6
5
4
3
2


Fig. 3

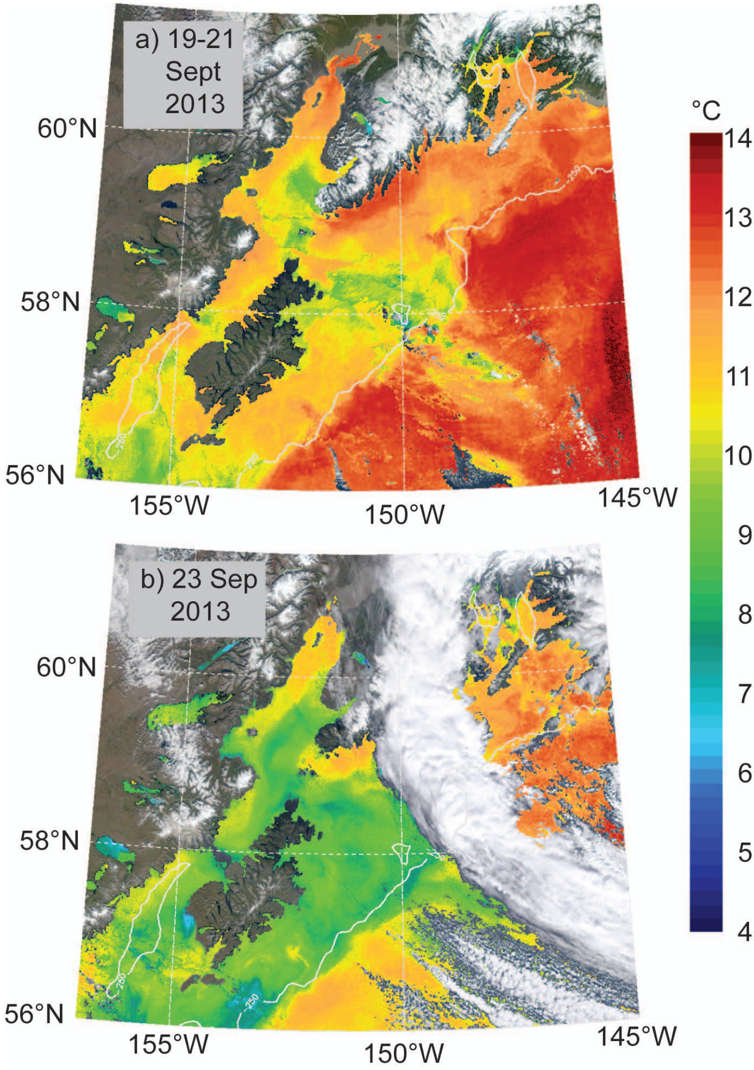
a) 19-21 Sept 2013
b) 23 Sep 2013
60°N
58°N
56°N
155°W
150°W
145°W
°C
14
13
12
11
10
9
8
7
6
5
4

Fig. 4

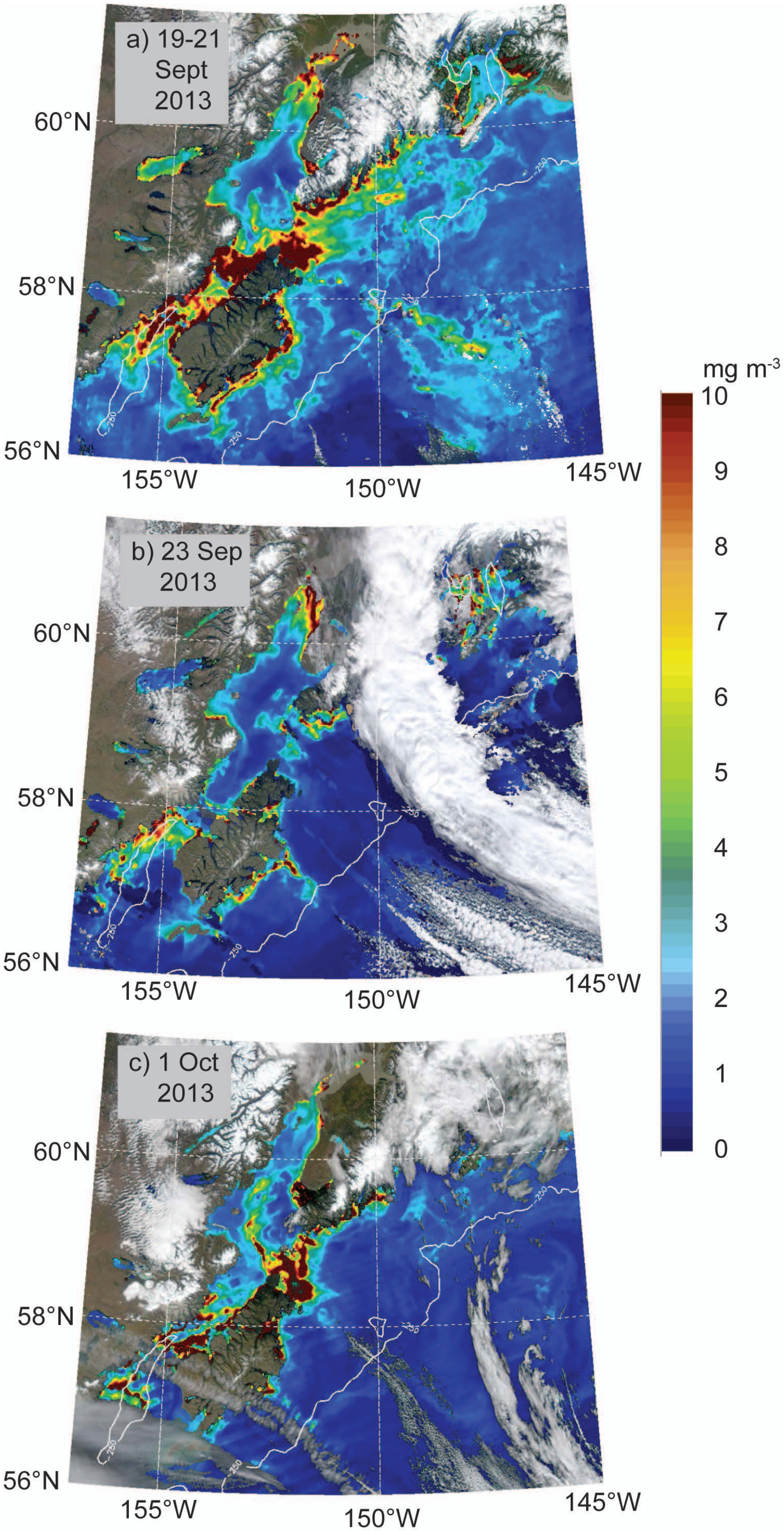
a) 19-21 Sept 2013
b) 23 Sep 2013
c) 1 Oct 2013
60°N
58°N
56°N
155°W
150°W
145°W
-250
mg m-3
10
9
8
7
6
5
4
3
2
1
0

Fig. 5

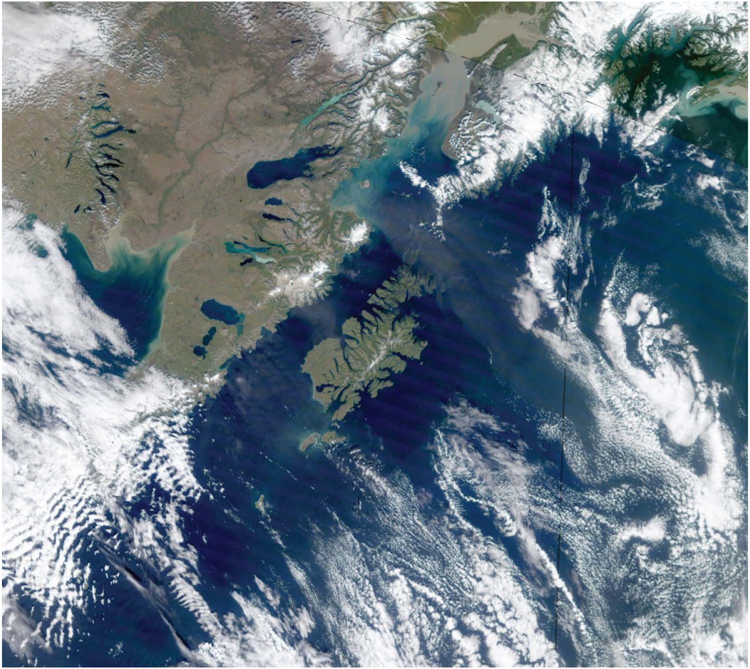

Fig. 6

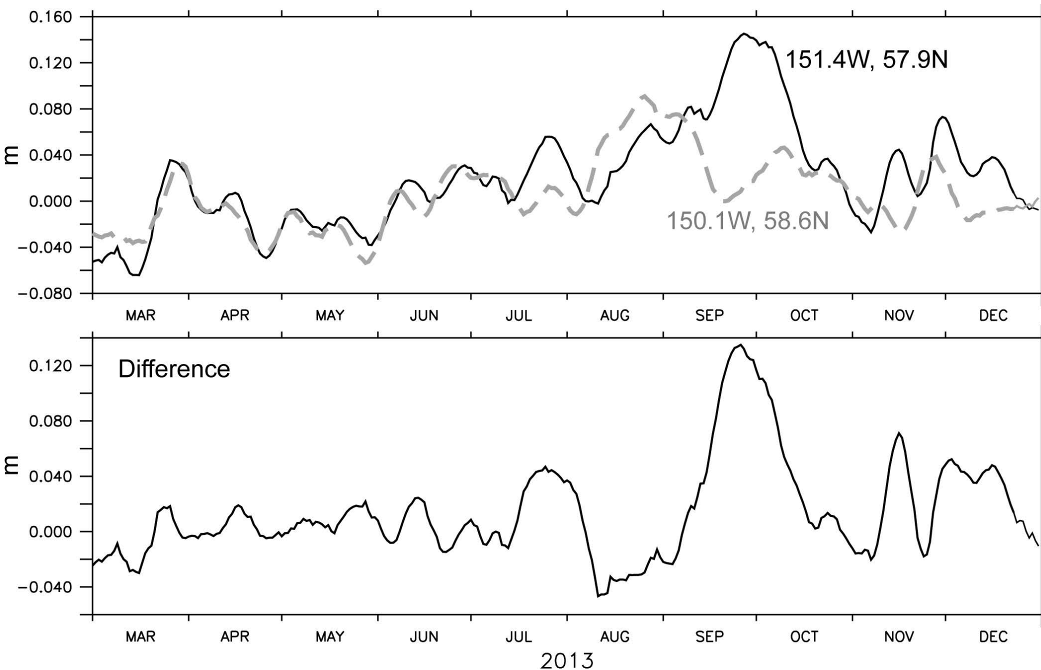
0.160
0.120
0.080
0.040
0.000
−0.040
−0.080
m
151.4W, 57.9N
150.1W, 58.6N
MAR
APR
MAY
JUN
JUL
AUG
SEP
OCT
NOV
DEC
Difference
0.120
0.080
0.040
0.000
−0.040
m
MAR
APR
MAY
JUN
JUL
AUG
SEP
OCT
NOV
DEC
2013

Fig. 7

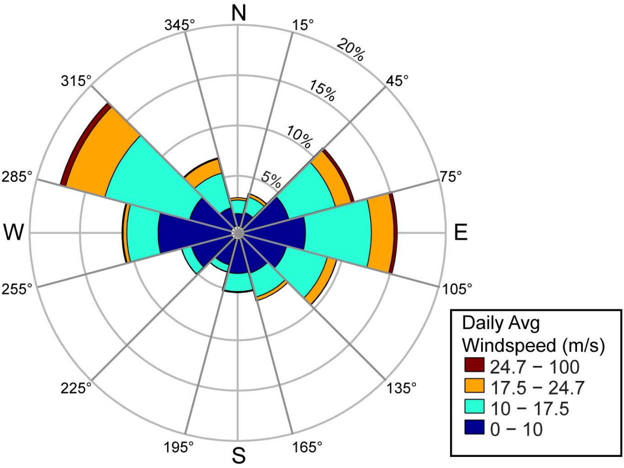
N
345°
15°
20%
315°
15%
45°
10%
285°
5%
75°
W
E
255°
105°
225°
135°
195°
S
165°
Daily Avg
Windspeed (m/s)
24.7 – 100
17.5 – 24.7
10 – 17.5
0 – 10

Fig. 8

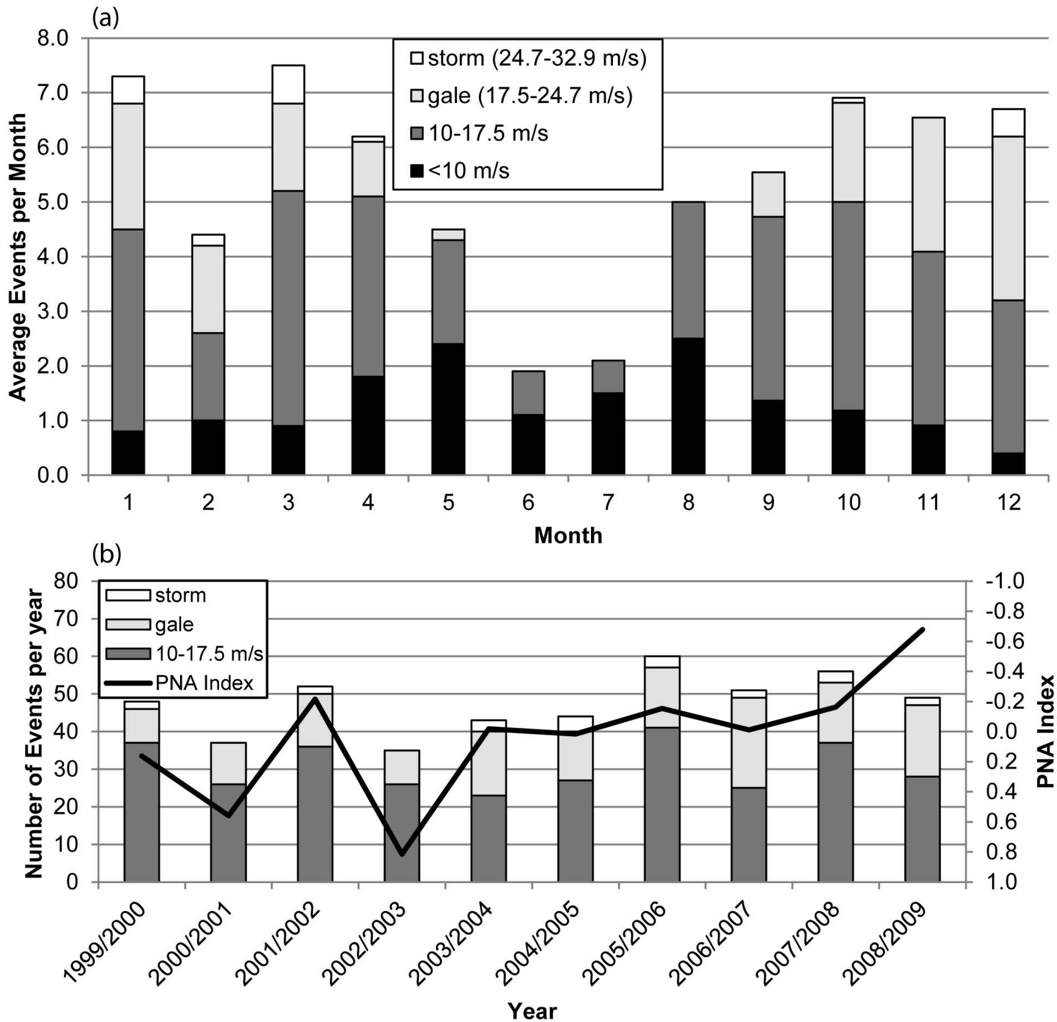

(a)
Average Events per Month
storm (24.7-32.9 m/s)
gale (17.5-24.7 m/s)
10-17.5 m/s
<10 m/s
8.0
7.0
6.0
5.0
4.0
3.0
2.0
1.0
0.0
1
2
3
4
5
6
7
8
9
10
11
12
Month
(b)
Number of Events per year
storm
gale
10-17.5 m/s
PNA Index
80
70
60
50
40
30
20
10
0
-1.0
-0.8
-0.6
-0.4
-0.2
0.0
0.2
0.4
0.6
0.8
1.0
PNA Index
1999/2000
2000/2001
2001/2002
2002/2003
2003/2004
2004/2005
2005/2006
2006/2007
2007/2008
2008/2009
Year


Fig. 9

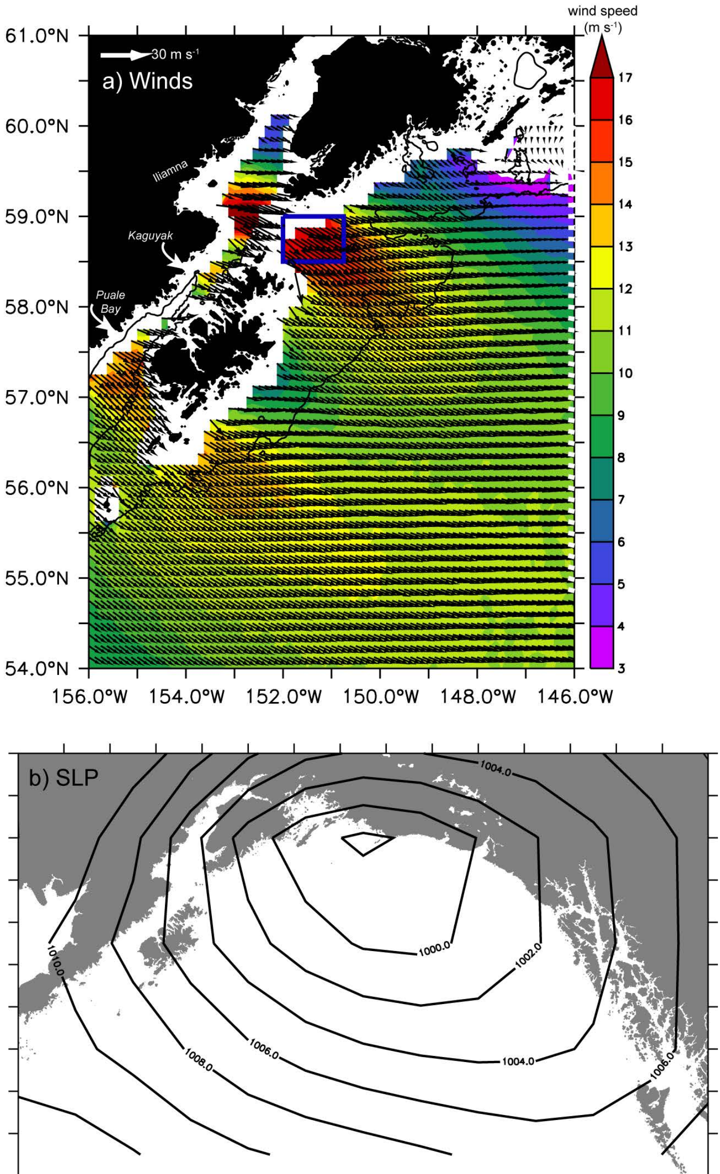

wind speed (m s-1)
30 m s-1
a) Winds
Iliamna
Kaguyak
Puale Bay
61.0°N
60.0°N
59.0°N
58.0°N
57.0°N
56.0°N
55.0°N
54.0°N
156.0°W
154.0°W
152.0°W
150.0°W
148.0°W
146.0°W
b) SLP
1000.0
1002.0
1004.0
1006.0
1008.0
1010.0
62.0°N
52.0°N
158°W
154°W
150°W
146°W
142°W
138°W
134°W


Fig. 10

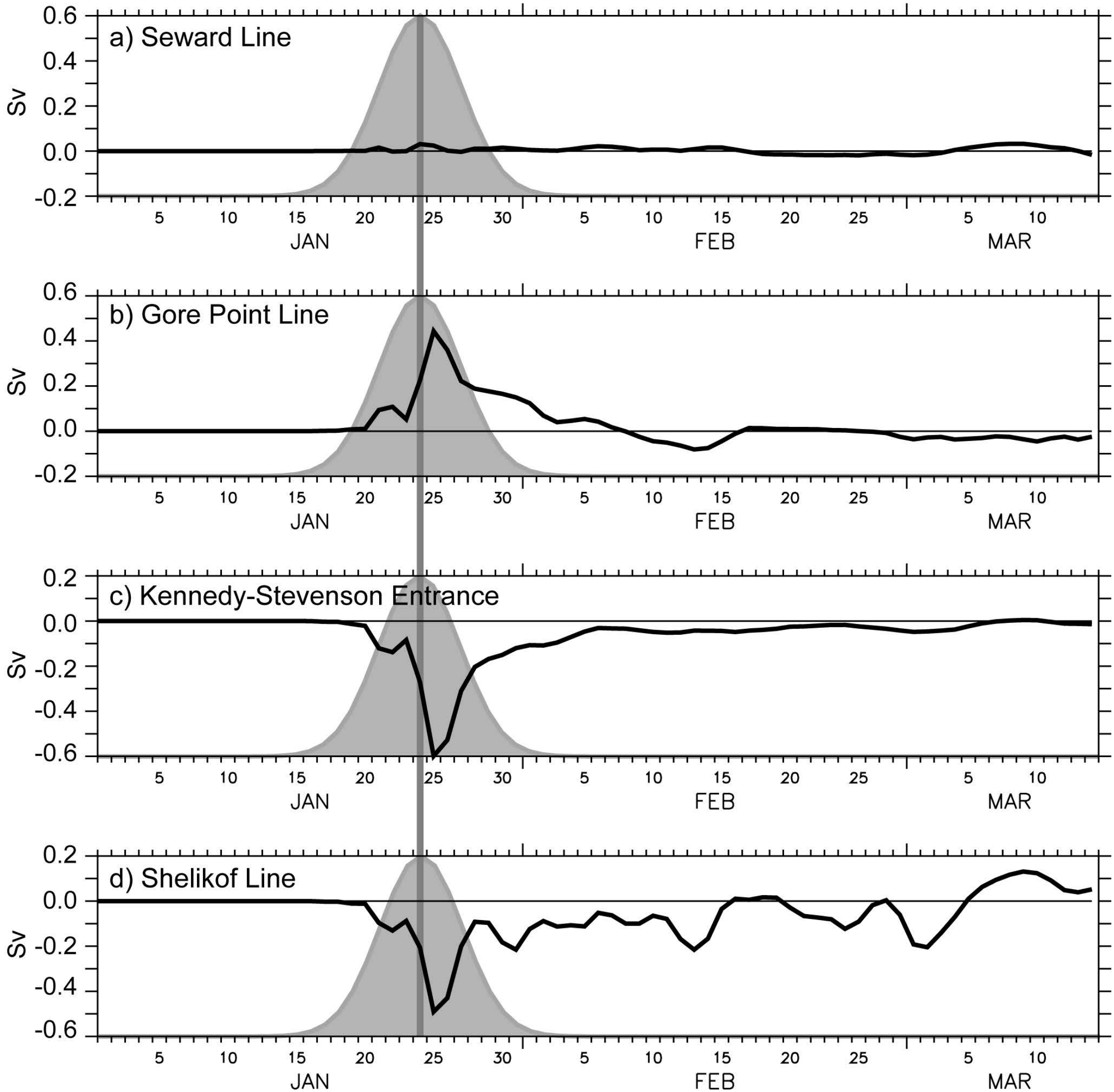
a) Seward Line
b) Gore Point Line
c) Kennedy-Stevenson Entrance
d) Shelikof Line
Sv
0.6
0.4
0.2
0.0
-0.2
-0.4
-0.6
5
10
15
20
25
30
JAN
FEB
MAR

Fig. 11

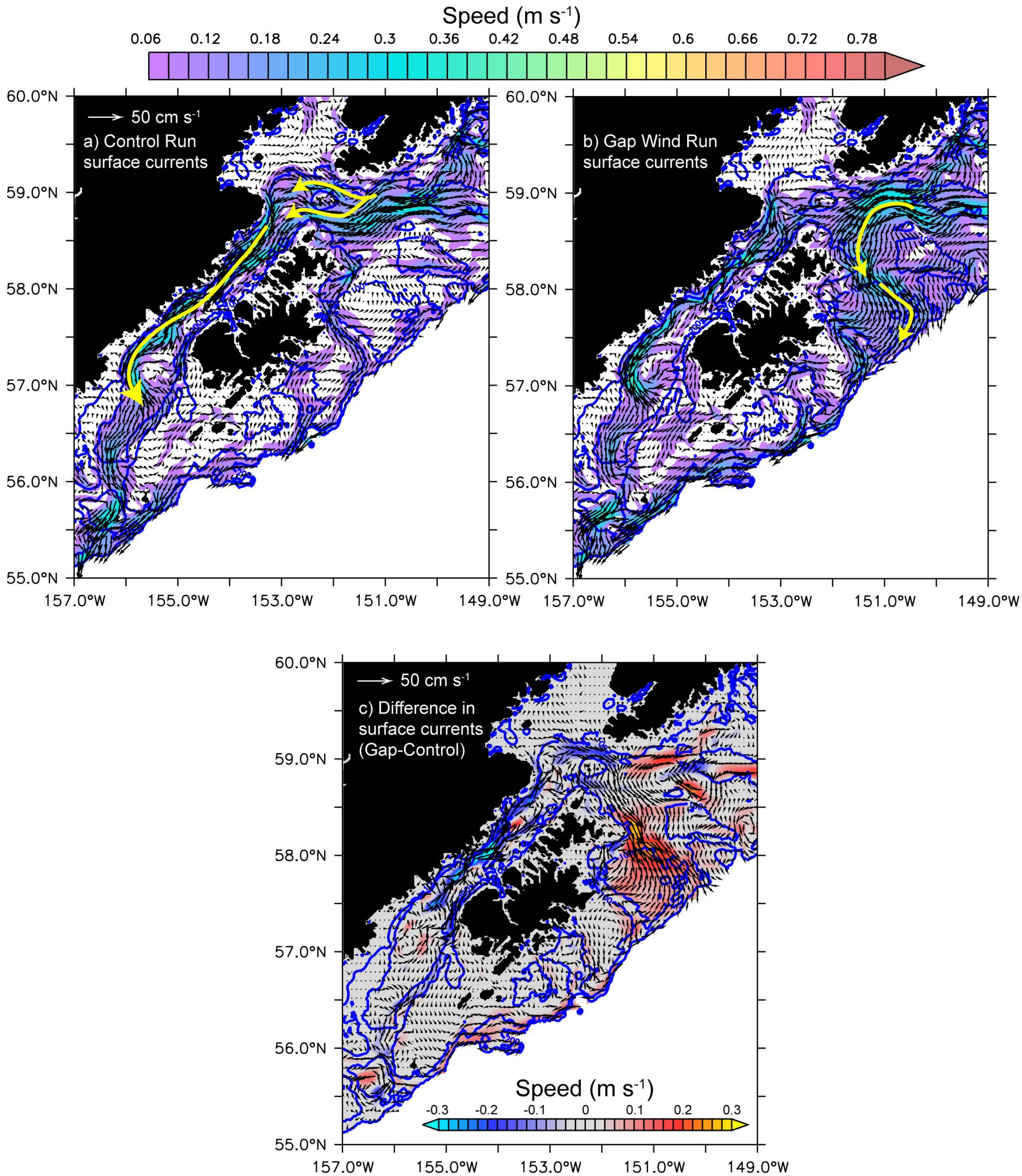

Speed (m s-1)
0.06
0.12
0.18
0.24
0.3
0.36
0.42
0.48
0.54
0.6
0.66
0.72
0.78
50 cm s-1
a) Control Run
surface currents
b) Gap Wind Run
surface currents
60.0°N
59.0°N
58.0°N
57.0°N
56.0°N
55.0°N
157.0°W
155.0°W
153.0°W
151.0°W
149.0°W
50 cm s-1
c) Difference in
surface currents
(Gap-Control)
Speed (m s-1)
-0.3
-0.2
-0.1
0
0.1
0.2
0.3


Fig. 12

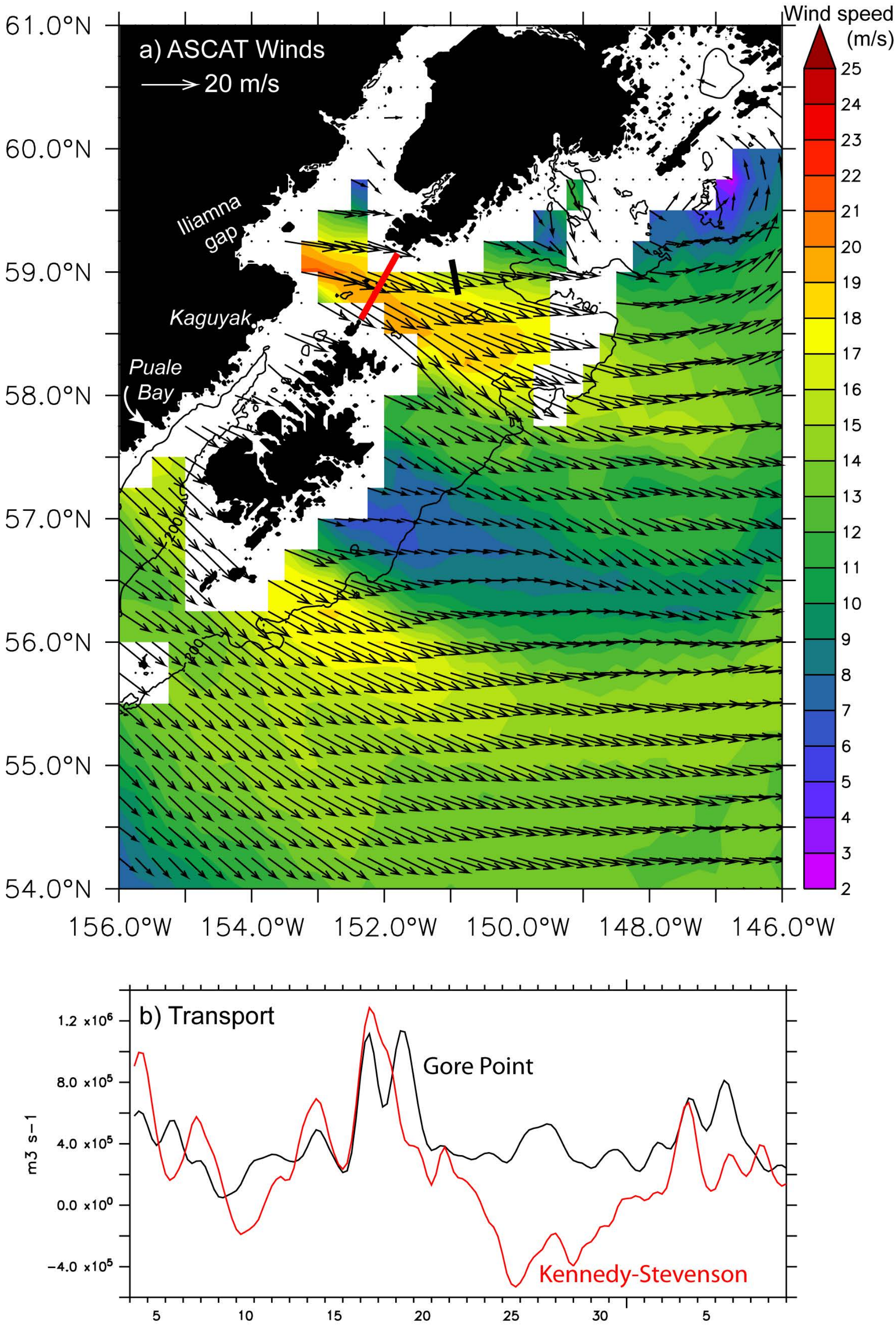

a) ASCAT Winds
20 m/s
Wind speed (m/s)
Iliamna gap
Kaguyak
Puale Bay
200
61.0°N
60.0°N
59.0°N
58.0°N
57.0°N
56.0°N
55.0°N
54.0°N
156.0°W
154.0°W
152.0°W
150.0°W
148.0°W
146.0°W
25
24
23
22
21
20
19
18
17
16
15
14
13
12
11
10
9
8
7
6
5
4
3
2
b) Transport
Gore Point
Kennedy-Stevenson
m3 s−1
1.2 x10^6
8.0 x10^5
4.0 x10^5
0.0 x10^0
−4.0 x10^5
5
10
15
20
25
30
5
MAY
JUN


Fig. 13

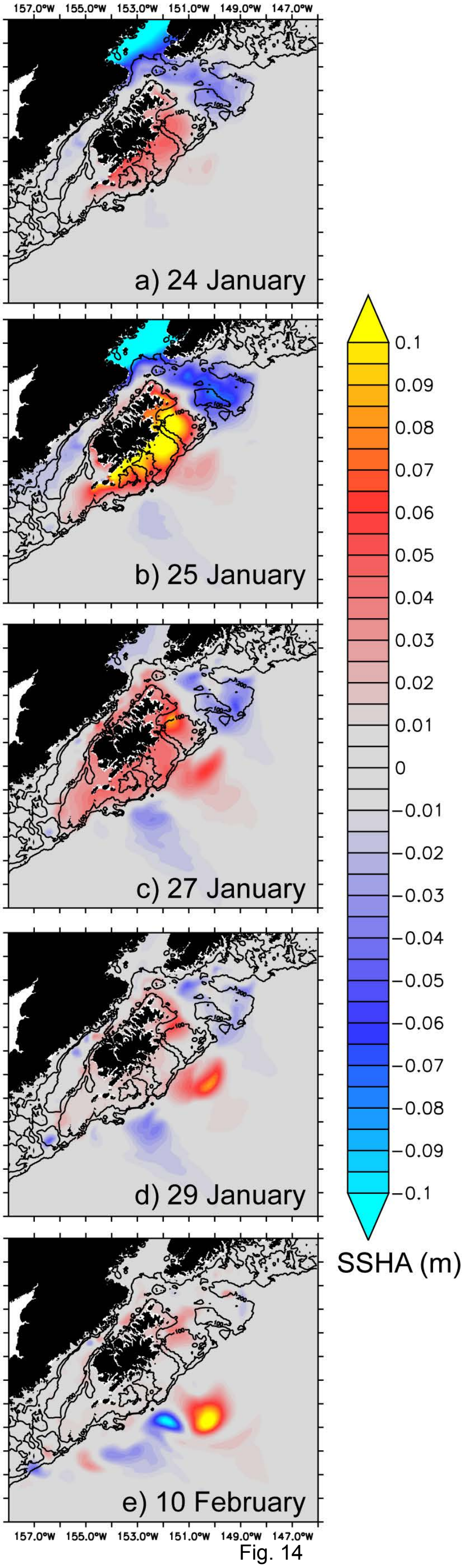

157.0°W
155.0°W
153.0°W
151.0°W
149.0°W
147.0°W
60.0°N
59.0°N
58.0°N
57.0°N
56.0°N
55.0°N
54.0°N
a) 24 January
b) 25 January
c) 27 January
d) 29 January
e) 10 February
0.1
0.09
0.08
0.07
0.06
0.05
0.04
0.03
0.02
0.01
0
−0.01
−0.02
−0.03
−0.04
−0.05
−0.06
−0.07
−0.08
−0.09
−0.1
SSHA (m)

Fig. 14